Development of Prodrug 4-Chloro-3-(5-methyl-3-{[4-(2-pyrrolidin-1-ylethoxy)phenyl]amino}-1,2,4-benzotriazin-7-yl)phenyl Benzoate (TG100801): A Topically Administered Therapeutic Candidate in Clinical Trials for the Treatment of Age-Related Macular Degeneration

Moorthy S. S. Palanki,*[,†] Hideo Akiyama,[‡] Peter Campochiaro,[‡] Jianguo Cao,[†] Chun P. Chow,[†] Luis Dellamary,[†] John Doukas,[†] Richard Fine,[§] Colleen Gritzen,[†] John D. Hood,[†] Steven Hu,[†] Shu Kachi,[‡] Xinshan Kang,[§] Boris Klebansky,[§] Ahmed Kousba,[†] Dan Lohse,[†] Chi Ching Mak,[†] Michael Martin,[†] Andrew McPherson,[†] Ved P. Pathak,[†] Joel Renick,[†] Richard Soll,[†] Naoyasu Umeda,[‡] Shiyin Yee,[†] Katsutoshi Yokoi,[‡] Binqi Zeng,[†] Hong Zhu,[†] and Glenn Noronha[†]

TargeGen, Inc., 9380 Judicial Drive, San Diego, California 92121, Department of Ophthalmology, Johns Hopkins Hospital School of Medicine, 719 Maumenee, 600 N. Wolfe Street, Baltimore, Maryland 21287, and BioPredict, Inc., 660 Kinderkamack Road, Oradell, New Jersey 07649

Received September 11, 2007

Age-related macular degeneration (AMD) is one of the leading causes of loss of vision in the industrialized world. Attenuating the VEGF signal in the eye to treat AMD has been validated clinically. A large body of evidence suggests that inhibitors targeting the VEGFr pathway may be effective for the treatment of AMD. Recent studies using Src/YES knockout mice suggest that along with VEGF, Src and YES play a crucial role in vascular leak and might be useful in treating edema associated with AMD. Therefore, we have developed several potent benzotriazine inhibitors designed to target VEGFr2, Src, and YES. One of the most potent compounds is 4-chloro-3-{5-methyl-3-[4-(2-pyrrolidin-1-yl-ethoxy)phenylamino]benzo[1,2,4]triazin-7-yl}phenol (**5**), a dual inhibitor of both VEGFr2 and the Src family (Src and YES) kinases. Several ester analogues of **5** were prepared as prodrugs to improve the concentration of **5** at the back of the eye after topical administration. The thermal stability of these esters was studied, and it was found that benzoyl and substituted benzoyl esters of **5** showed good thermal stability. The hydrolysis rates of these prodrugs were studied to analyze their ability to undergo conversion to **5** in vivo so that appropriate concentrations of **5** are available in the back-of-the-eye tissues. From these studies, we identified 4-chloro-3-(5-methyl-3-{[4-(2-pyrrolidin-1-ylethoxy)phenyl]amino}-1,2,4-benzotriazin-7-yl)phenyl benzoate (**12**), a topically administered prodrug delivered as an eye drop that is readily converted to the active compound **5** in the eye. This topically delivered compound exhibited excellent ocular pharmacokinetics and poor systemic circulation and showed good efficacy in the laser induced choroidal neovascularization model. On the basis of its superior profile, compound **12** was advanced. It is currently in a clinical trial as a first in class, VEGFr2 targeting, topically applied compound for the treatment of AMD.

Introduction

In the industrialized world, the leading causes of vision loss are diabetic retinopathy and age-related macular degeneration (AMD).[1] In both conditions, up-regulation of vascular endothelial growth factor (VEGF) leads to vascular dysfunction.[2–4] In patients with diabetes, chronic hyperglycemia causes damage to vascular cells in the retina, resulting in capillary drop out and retinal ischemia. Retinal ischemia causes increased production of VEGF,[5,6] which promotes growth of new vessels along the surface of the retina (retinal neovascularization) and also causes pre-existent retinal vessels to become leaky. The development of retinal neovascularization heralds the onset of proliferative diabetic retinopathy, which often leads to blindness if untreated. The excessive leakage of plasma from pre-existent retinal vessels causes collection of fluid in the interstitial space of the macula, which is referred to as diabetic macular edema (DME). Collection of fluid in the macula causes loss of vision that is initially reversible if the leakage can be stopped, but if the edema is prolonged, structural damage occurs to retinal cells resulting in permanent loss of vision.

In patients with AMD, a combination of oxidative damage and complement-mediated damage causes degeneration of photoreceptors and retinal pigmented (RPE) cells and gradual loss of vision. This gradual degeneration is generally referred to as "dry AMD" and by mechanisms that are not completely understood leads to up-regulation of VEGF in RPE cells, which in 20% of patients is sufficient to cause growth of neovascularization from the choroid into the sub-RPE and subretinal spaces (choroidal neovascularization) commonly referred to as "wet AMD". Choroidal neovascularization tends to occur in the macula and is made up of fenestrated vessels that leak plasma causing subretinal and intraretinal fluid resulting in sudden loss of vision. As is the case with DME, the loss of vision from collection of excess fluid beneath and/or within the macula is initially reversible, but unless it is eliminated in a timely fashion, permanent visual loss occurs.

Thus, VEGF-induced vascular leakage plays a central role in the vision loss associated with diabetic retinopathy and AMD.[7–10] Ranibizumab (Lucentis TM, Genentech, South San Francisco, CA) is a humanized antigen binding fragment (Fab) that binds all isoforms of VEGF-A.[11] Monthly intraocular injections of ranibizumab caused significant visual improvement in patients with choroidal neovascularization due to AMD[12,13] and DME.[14] Bevacizumab, a humanized full-length monoclonal antibody that binds all isoforms of VEGF-A, has been approved for the treatment of colon cancer[15] but has also been given off-

* To whom correspondence should be addressed. Phone: +1-858-964-2136. Fax: +1-858-678-0762. E-mail: Palanki@targegen.com.
† TargeGen, Inc.
‡ Johns Hopkins Hospital School of Medicine.
§ BioPredict, Inc.

10.1021/jm7011276 CCC: $40.75
Published on Web 02/27/2008

Table 1. Structures of Benzotriazine Analogues and in Vitro Activities in Src and VEGFr2

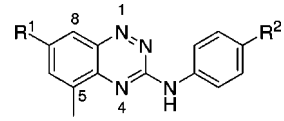

compd	R^1	R^2	IC_{50}, nM		
			Src	VEGFr2	YES
1	Ph	4-(2-pyrrolidin-1-ylethoxy)	340	530	110
2	2-chlorophenyl	4-(2-pyrrolidin-1-ylethoxy)	35	1900	22
3	2,6-dimethylphenyl	4-(2-pyrrolidin-1-ylethoxy)	7	560	1.2
4	2,6-dichlorophenyl	4-(2-pyrrolidin-1-ylethoxy)	14	130	10
5	2-chloro-5-hydroxyphenyl	4-(2-pyrrolidin-1-ylethoxy)	1.8	2.2	0.3
6	2-chloro-5-hydroxyphenyl	4-(2-pyrrolidin-1-ylethylaminosulfonyl)	3.6	4.7	1.3
7	2-chloro-5-hydroxyphenyl	4-(piperazin-1-ylcarbonyl)	3.6	1.8	5.2
8	2-chloro-5-hydroxyphenyl	4-(piperidin-4-ylsulfonyl)	5.2	1.7	4.1
9	2-chloro-5-hydroxyphenyl	4-(3-pyrrolidin-1-ylpropyl)	1.5	2.7	4.8

label by intraocular injection in patients with ocular diseases.[16] Intraocular injections are tolerated fairly well, but they carry some risks of infection and retinal detachment, and the more injections a patient receives, the greater is the risk. Also, returning for retinal examinations and possible injections every month is a hardship on many patients. Therefore, development of VEGF antagonists that can be delivered by less invasive means is a major priority for the treatment of AMD.[17–23]

Among angiogenic growth factors, the unique role of VEGF in disrupting endothelial barrier function has been established. Injection of exogenous VEGF into the eye of mice lacking Src or YES ($Src^{-/-}$ or $YES^{-/-}$) did not compromise the endothelial barrier function clearly establishing a link between VEGF and Src in vascular leak.[24] Studies using chick embryos demonstrated that Src activity induced the coupling of focal adhesion kinase (FAK) to integrin $\alpha_v\beta_5$, an important process in the VEGF-mediated signaling event in chick embryo blood vessels.[25] When healthy mice were injected with VEGF intravitreally, the leakage of blood and serum into the retina and the vitreous was observed. However, intravitreal injection of VEGF to Src knockout mice did not result in the leakage of blood and serum establishing the role of Src in these disease conditions.[26] Apart from its role in AMD, Src is also known to be involved in oncology, osteopetrosis, and the matrix signaling pathway necessary for the maturation of osteoclasts.[27] These results demonstrate that while VEGF plays a critical role in macular degeneration, Src and YES also play an important role in maintaining vascularity and the endothelial barrier.[28] Hence, we believe that small molecules targeting VEGFr, Src, and YES might offer a better therapeutic advantage over agents targeting VEGFr alone. Since both VEGF and Src are involved in several biological processes, topical application of drug to a local site might negate the side effects due to systemic circulation of an inhibitor.

We focused on developing compounds that can be administered topically as eye drops and reach the back of the eye in sufficient concentrations for the treatment of back-of-the eye diseases, as in the case of AMD. In the case of AMD, therapeutically effective concentrations of a drug should be achieved in the sclera, choroid, and potentially the retina. It is also equally important that if the drug enters the systemic circulation, it should be cleared rapidly to lower the risk of accumulation and allay potential systemic effects. No compound in the market at present achieves these goals, and topical eye-drop delivery for back-of-the-eye disease is viewed with some skepticism because of the unique nature of the eye and the paucity of a systematic body of work, where back-of-the-eye tissues have been targeted and adequate drug level or therapeutic effect by topical delivery has been demonstrated.

We have recently disclosed a series of substituted benzotriazines as potent inhibitors of Src kinase,[29] and we have shown the potential utility of these compounds by demonstrating their activity in preclinical animal disease models of cancer.[30] We designed these benzotriazines to potently inhibit Src, YES kinases, and VEGFr. Here, we present our efforts in optimizing the benzotriazine series starting with analogue **1** for its biochemical potency against VEGFr, Src, and YES. We also describe the further optimization of a subset of these benzotriazines to enhance ocular pharmacokinetics and to minimize systemic exposure, both of which we view as critical for a chronic therapy where localized effects in the eye are the target. We demonstrate that compound **12** is active in preclinical models when administered topically as an eye drop.

Chemistry

The compounds collated in Table 1 were prepared as shown in Scheme 1. 4-Bromo-6-methyl-2-nitroaniline (**21**) was reacted with cyanamide and pyridine hydrochloride to give an intermediate guanidine. The guanidine was cyclized with 30% aqueous sodium hydroxide to give the 1-oxobenzotriazine **22**.[31,32] The oxobenzotriazine **22** was reduced using Raney nickel and hydrogen in ethanol to give 3-amino-7-bromobenzotriazine **23** in good yield. Various aryl 7-substituted benzotriazines (**24a**−**e**) were prepared by treating 3-amino-7-bromo-5-methylbenzotriazine (**23**) with arylboronic acids such as 2-chloro-5-methoxyphenylboronic acid, phenylboronic acid, 2-chlorophenylboronic acid, 2,6-dimethylphenylboronic acid, and 2,6-dichlorophenylboronic acid to give **24a**−**e**, respectively, in good yield (50−70%) under Suzuki coupling conditions.[33] The advanced intermediates (**24b**−**e**) were treated with 4-(2-pyrrolidin-1-ylethoxy)bromobenzene (**25a**) under Buchwald−Hartwig cross-coupling reaction conditions using palladium and Xantphos to afford compounds **1**–**4**, respectively.[34] Similarly, the treatment of **24a** with various aryl bromides (**25a**−**e**) under Buchwald−Hartwig cross-coupling reaction conditions using palladium and Xantphos resulted in the intermediates (**26a**−**e**), respectively. The methoxy group in **26a**−**e** was cleaved using boron tribromide to give phenol analogues **5**–**9**.

The synthesis of the compounds collected in Table 2 is shown in Scheme 2. The treatment of **5** with acetyl chloride, isopropionyl chloride, benzoyl chloride, 4′-methylbenzoyl chloride, 2,2-dimethylpropionyl chloride, nicotinoyl chloride, 2,6-dimethylbenzoyl chloride, and 2,6-dichlorobenzoyl chloride resulted in compounds **10**, **11**, **12**, **13**, **14**, **17**, **18**, and **19**, respectively.

Scheme 1[a]

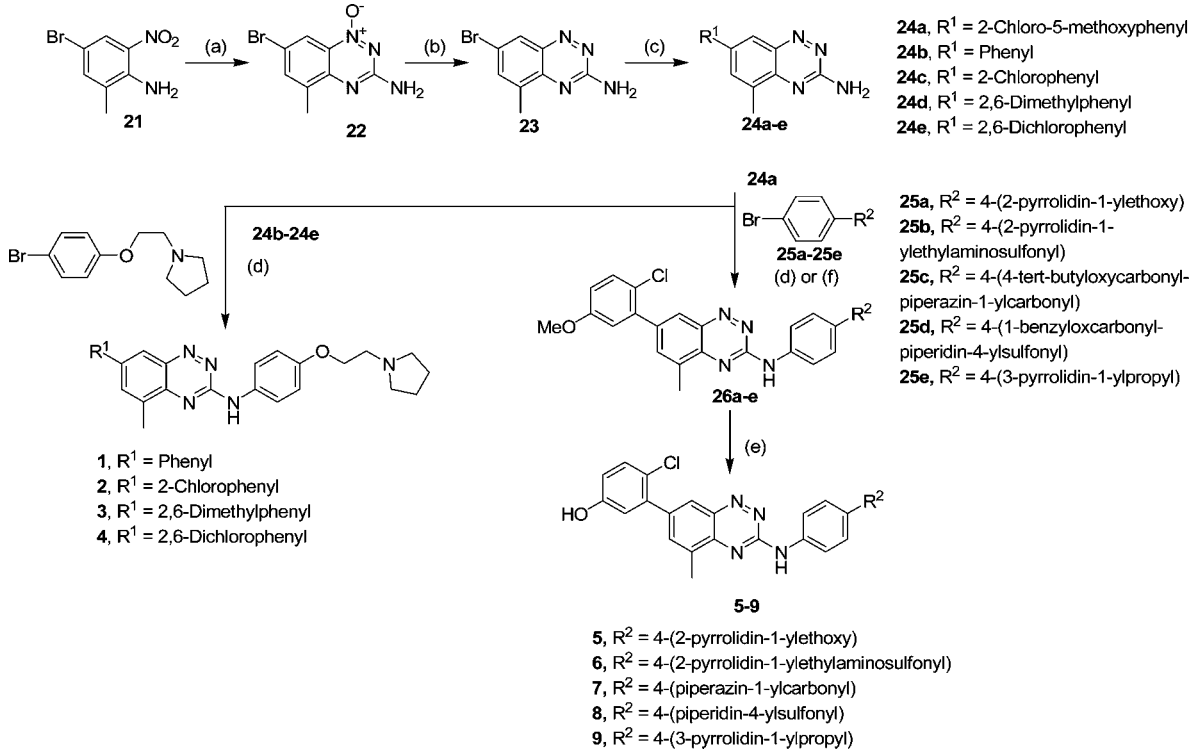

[a] (a) (i) NH_2CN, pyridine HCl, 100 °C, 12 h; (ii) 30% aqueous NaOH, 100 °C, 2 h; (b) 10% Raney nickel, H_2, EtOH, room temp, 12 h; (c) $R^1B(OH)_2$, $Pd(PPh_3)_4$, Na_2CO_3, DME/EtOH/H_2O, reflux, 12 h; (d) $Pd_2(dba)_3$, Xantphos, Cs_2CO_3, dioxane, reflux, 12 h; (e) BBr_3, DCM, 0 °C to room temp; (f) $Pd(OAc)_2$, Xantphos, K^+t-BuO^-, dioxane, reflux, 12 h.

Table 2. Stability of Prodrugs of **5**[a]

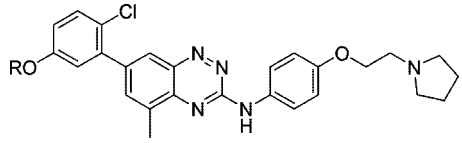

compd	R	chem stability under autoclave conditions, %	hydrolysis rate in rabbit eye homogenate, (ng/mL)/h
5	H	stable	ND
10	CH_3CO	<20	ND
11	$(CH_3)_2CO$	~50	ND
12	PhCO	>90	288
13	*p*-MePhCO	>90	ND
14	*t*-BuCO	>90	172
15	Na_2PO_3	<20	ND
16	NH_2CH_2CO	<20	ND
17	Nicotinoyl	~50	ND
18	2,6-Dimethylbenzoyl	>90	1.1
19	2,6-Dichlorobenzoyl	>90	1.7
20	4-(morpholin-4-ylmethyl)benzoyl	>90	ND

[a] The thermal stability of these prodrugs were measured at 120 °C for 1 h. The compounds that were stable to high temperature were selected and studied in rabbit eye homogenate for their ability to undergo hydrolysis to release **5**. ND = not determined.

Disodium phosphate analogue **15** was prepared from **5** by treating it with phosphorus oxychloride in the presence of triethylamine in dichloromethane, followed by sodium bicarbonate at room temperature. Glycinate analogue **16** was prepared by carbodiimide coupling of **5** with *tert*-butoxycarbonylaminoacetic acid, followed by the deprotection of butyloxycarbonyl using 5% trifluoroacetic acid in dichloromethane at room temperature. Compound **20** was also prepared by carbodiimide coupling of **5** with 4-(morpholin-4-ylmethyl)benzoic acid at room temperature.

Scheme 2[a]

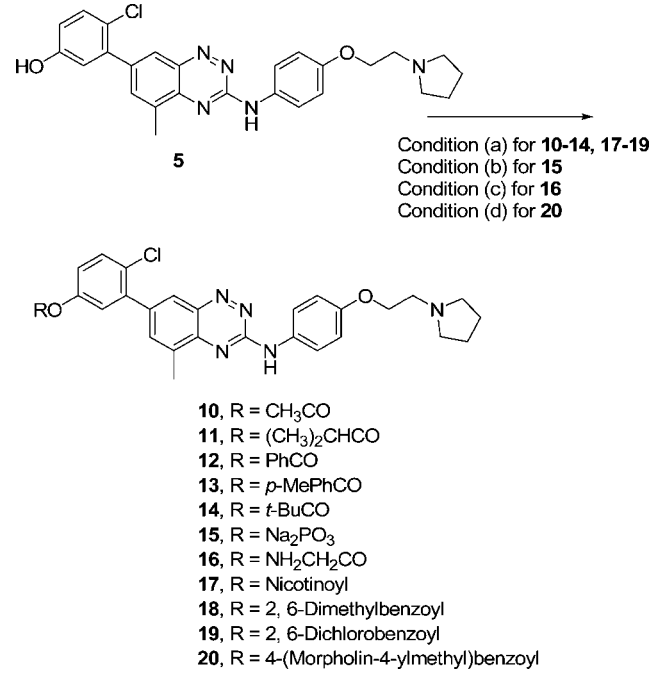

[a] (a) RCl, Et_3N, DCM, room temp; (b) (i) $POCl_3$, Et_3N, DCM, room temp; (ii) $NaHCO_3$, room temp; (c) (i) *tert*-butoxycarbonylaminoacetic acid, EDCI, DMAP, DMF, room temp; (ii) 5% TFA/DCM, room temp; (d) 4-(morpholin-4-ylmethyl)benzoic acid, EDCI, DMAP, DMF, room temp.

Results and Discussion

For clarity of discussion, only a selected group of compounds are shown in Tables 1 and 2 to describe the results of the

structure−activity relationship studies. The 7-phenyl substituted analogue **1** showed modest inhibitory activity against both Src (IC_{50} = 340 nM) and VEGFr2 (IC_{50} = 530 nM). The introduction of a single chloro group at the 2-position of the 7-phenyl ring resulted in approximately a 10-fold increase in the activity against Src but resulted in a 4-fold drop in potency against VEGFr2 as seen with compound **2**. The introduction of two methyl groups at the 2 and 6 positions of the 7-phenyl group resulted in **3**, which increased its potency against Src (IC_{50} = 7 nM) compared to **2**. Similarly compound **3** showed approximately 4-fold improvement in potency against VEGFr2 (IC_{50} = 560 nM). The potency was improved approximately 4-fold against both Src and VEGFr2 when the dimethyl groups on the 7-phenyl ring were replaced with dichloro groups as shown in **4**. While compound **4** has acceptable biochemical potency against Src, it is 9 times weaker against VEGFr2. Consistent with earlier studies, the introduction of small hydrophobic ortho substituents on the phenyl ring orients this group perpendicular to the benzotriazine, resulting in improved binding with Src and VEGFr2.[29] Chloro substituents at the ortho position improve potency against VEGFr2.

Further lead optimizations were carried out with the aid of molecular modeling studies. At the time the work was started, there was no crystal structure available for fully activated Src. As such, a homology model of activated Src was constructed on the basis of the activated crystal structure of Lck.[35] Crystal structures for fully activated VEGFr2 were available from the outset of work.[36] Figure 1A depicts the binding of **2** at the ATP binding pocket of Src. The 2-chlorophenyl group was bound deep inside a hydrophobic pocket near the αC-helix. Glu310 located on the αC-helix and available only upon activation was in proximity to the phenyl group. The benzotriazine ring interacts with the ATP binding hinge region. We noticed that compound **2** in VEGFr2 was binding in a similar fashion to **2** in Src. The 2-chlorophenyl group is in proximity to Glu885 from the αC-helix in VEGFr2 (Figure 1B). We therefore designed molecules with a donor moiety to interact with Glu310 in Src and Glu885 in VEGFr2 to enhance potency. On the basis of earlier lead optimization efforts, we decided to focus our initial efforts on the hydrophobic pocket where the 7-(2-chlorophenyl) group binds. We observed that Glu310 located on the αC helix deep within the hydrophobic pocket orients the carboxylic acid group of Glu310 toward the inside of the hydrophobic pocket in proximity to the 7-phenyl group. We envisioned that one could take advantage of this carboxylic group by incorporating a donor group at the 5-position of the 7-(2-chlorophenyl) group of **2**. This donor would potentially interact with the carboxylic acid and enhance its potency further (Figure 1C). Compound **5** was designed on the basis of these design ideas suggested by the homology model. Similar homology modeling studies using a VEGFr model also revealed that Glu883 on the αC-helix near the hydrophobic pocket orients the carboxylic group toward the meta position of the 7-phenyl ring. Homology modeling also showed that compound **5** binds to the ATP pocket of VEGFr2 in a similar fashion to the binding mode seen in Src and the hydroxy group of **5** interacts with Glu883 (Figure 1D). Modeling studies suggested that the hydroxyl group on the meta position of the 7-phenyl ring increases the potency of **5** toward both Src and VEGFr2 via these Glu hydrogen-bonding interactions. Interactions with this Glu deep within this hydrophobic pocket enhance dipole-charged interactions because of the low dielectric environment. This added interaction further stabilizes the activated form of Src. The concept of taking advantage of a carboxylic group buried deep within this hydrophobic pocket has been explored recently.[37] It is noted that the homology models have limitations in the sense that it is well-known that active sites of kinases have sufficient flexibility to accommodate inhibitors through induced fit. We have disclosed the complete details of this design strategy targeting Src and utilized the above concept in developing different structural classes of compounds, selectively targeting and optimizing against different kinases.[30,38]

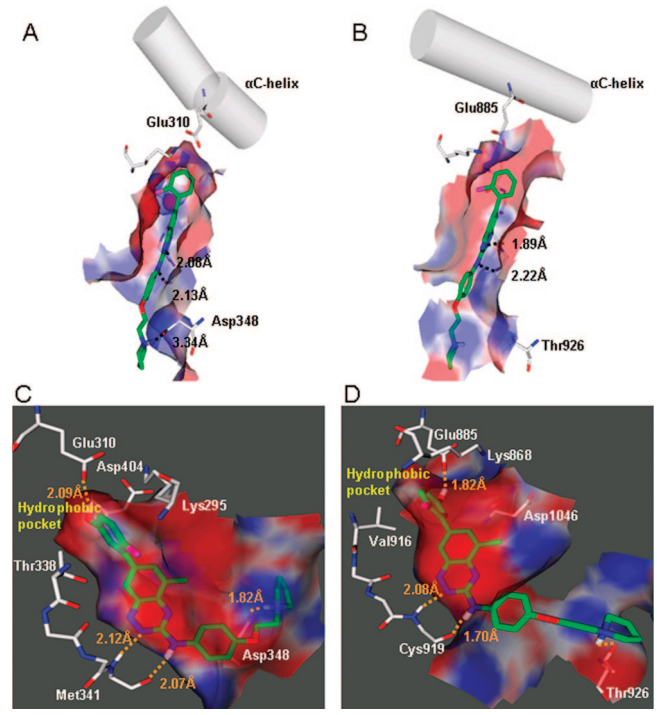

Figure 1. (A) Compound **2** at the ATP pocket of Src. The Glu310 from αC-helix is in proximity to the 7-phenyl ring. (B) Compound **2** at the ATP pocket of VEGFr2. The Glu885 from the αC-helix is in proximity to the 7-phenyl ring. (C) Compound **5** at the ATP pocket of Src. (D) Compound **5** at the ATP pocket of VEGFr2. The molecular surface is colored according to the hydrophobicity of the surrounding residues; blue is hydrophilic, and red is hydrophobic. The hydroxyl group of **5** acts as hydrogen bond donor and interacts with Glu310 in Src (C). The binding orientation of **5** in the VEGFr pocket is very similar to that of **5** in Src (D). There are two hydrogen bond interactions between the benzotriazine ring and Cys919 that serves as the hinge. The hydroxyl group on **5** acts as hydrogen bond donor and interacts with Glu885.

Figure 1C depicts a minimized binding mode of a benzotriazine inhibitor **5** in the ATP pocket of the activated Src model, and the binding interactions are summarized as follows. The 7-substituted phenyl ring binds in the hydrophobic back pocket, positioning this phenyl ring perpendicular to the benzotriazine core. Our earlier studies[29] showed that a limited set of small hydrophobic groups may be substituted on this phenyl ring at very specific positions because the 7-phenyl binding pocket possesses a limited tolerance for larger groups. The 3-aminobenzotriazine moiety forms both donor and acceptor hydrogen bonds to Met341 in the hinge region, thus sharing a common site with the hinge binding purine ring of ATP. The 3-amino group from the benzotriazine core is attached to an aryl linker in a region of the ATP, which falls in the hydrophobic channel leading out toward a solvent accessible area. The spacer with a solublizing group binds in an area accessible to solvent. Benzotriazine inhibitors containing basic nitrogen in this region provide enhanced potency through protonation and interaction with Asp348.

Table 3. Exposure Levels of **5** in Ocular Tissues Following Single Bilateral Topical Instillation of **5** or **12** in Mice[a]

compd administered	compd measured	tissue	T_{max} (h)	C_{max} (μM)	AUC (h·μg/mL)
5	**5**	retina	0.5	3.6	3.2
		choroid/sclera	0.5	23	240
		cornea	0.5	64	560
		plasma	6	0.0020	NS
12	**12**	retina	24	5.3	63
		choroid/sclera	24	27	430
		cornea	24	3.7	55
		plasma	NS	NS	NS
12	**5**	retina	24	2.4	35
		choroid/sclera	24	29	540
		cornea	7	33	670
		plasma	24	0.0050	NS

[a] A 10 μL drop of **5** (70 μg, 137 nM) was instilled per eye to 20 male mice (C57BL/6). Similarly, a 10 μL drop of **12** (100 μg, 172 nM) was instilled per eye to 20 male mice (C57BL/6). Composite sampling was employed to generate tissue concentration−time profiles for **5** and **12** over the following time course (N = 4/time point): 0.5, 1, 3, 7, and 24 h postinstillation. Both eyes were removed from each mouse and dissected to obtain the cornea, retina, and eye cup (sclera and choroid). The maximum tissue concentrations of **5** were 3.6 and 23.4 μM for retinal and choroidal/sclera tissues, respectively, observed at 30 min postadministration for both tissues. Minimal system exposure (plasma concentrations, ≤2 nM) was observed for **5** following topical administration. Topical administration of **12** provided substantial posterior ocular tissue exposure to **5** and **12**. Conversion of **12** to the active **5** was observed in all ocular tissues. On the basis of total **5** tissue exposure (AUC_{0-24h}), the topical instillation of the prodrug formulation resulted in an 11-fold increase in retinal tissue exposure versus topical delivery of **5**. NS: insufficient data for calculation of pharmacokinetic parameters.

As anticipated, compound **5** showed improved potency toward both Src and VEGFr2. Compound **5** was 8 times more potent against Src and 60 times more potent against VEGFr2 compared to **2**. By keeping the 2-chloro-5-hydroxyphenyl group constant at the 7-position of the benzotriazine ring, we introduced several different groups at the R^2 position to further optimize this series. Compounds **6–9** showed equivalent potency to **5** with the designed donor interaction being the dominant driver of the potency. On the basis of the structure–activity relationship, compound **5** was selected for further studies.

It is known that upon stimulation with VEGF, the intracellular signals leading up to various mitogen activated map kinases and focal adhesion kinases are activated via Src family kinases, resulting in retinal microvascular endothelial cells (RMECs) dysregulation, proliferation, and differentiation in retinopathies. The ability of compound **5** to block VEGF-stimulated proliferation was evaluated in retinal microvascular endothelial cells (hRMVECs) in vitro. Compound **5** showed very good biochemical potency in Src, VEGFr2, and YES[39] biochemical assays. In this study, **5** was shown to inhibit hRMVEC cell proliferation, with an $IC_{50} = 610 \pm 72$ nM. This suggests that **5** has the therapeutic potential to inhibit VEGF function in ocular endothelial cells, a contributing factor to pathological angiogenesis in diseases such as AMD and PDR.[40]

Next, we examined the tissue levels of compound **5** in various parts of the eye to evaluate the compound's ability to penetrate to the back of the eye (Table 3). A dose of 70 μg (137 nmol) of **5** in 10 μL (0.7% w/v solution of **5** in 27% w/v PL90G formulation in water) was administered topically to an eye. The concentrations of **5** were measured at two different locations. A concentration of 23.4 μM (C_{max}) was reached in 30 min (T_{max} = 0.5 h) in the choroid and the sclera. However, the levels of compound **5** in the retina were relatively low ($AUC_{0-24h} = 3.2$ h·μg/mL). It is important for the compound to reach sufficient concentrations in the choroid and sclera in patients with AMD. However, in the case of patients with other blinding eye diseases (DME, for example), it is equally important for the drug to reach sufficient concentrations in the choroid and sclera as well as in the retina. The half-life of **5** in ocular tissues was very short; hence, the compound was administered topically minimum t.i.d. to maintain appropriate drug levels in the eye.[41] The maximum concentration one can achieve in formulations using compound **5** was 0.7% w/v. Further increase in concentration resulted in the precipitation of the material out of the solution. Since the compound solubility in the formulation was low, it was difficult to achieve the required concentration through a 10 μL drop. It is not advisable to administer a larger volume, since larger amount of the solution readily runs from the eyes, creating inconsistent results. Because of low levels of compound **5** in the retina, it was necessary to increase the frequency of administration to maintain sufficient levels in the eye. We also noticed that the increased frequency of administration of **5** caused irritation in the eyes of the animals. The eye irritation and low levels in retina coupled with short half-life ($T_{1/2} = 0.5$ h) made this compound less suitable for further development. One of the desirable properties of **5** is the lack of detectable levels in systemic circulation.

In order to attain adequate exposure of **5** in the relevant ocular tissues, followed by poor systemic levels, we decided to improve the back-of-the-eye tissue exposure levels of **5** through the preparation of prodrugs that masked the hydroxyl group. We reasoned that these ester prodrugs would be readily cleaved under physiological conditions to release the active drug in the eye.[42] It was anticipated that the prodrugs would have better and more sustained ocular exposure levels in the relevant back-of-the-eye tissues and would undergo hydrolysis to release the drug. It was also anticipated that if the prodrug or drug enters systemic circulation, it would be cleared very quickly, since **5** has rapid clearance when given systemically.

Several prodrugs were prepared and evaluated on the basis of two important criteria. First, in order to develop these compounds further, they have to be stable under thermal sterilization conditions. The prodrugs **10**−**20** (Table 2) were evaluated for their thermal stability at 120 °C for 1 h as a harsh accelerated test for thermal stability. The parent compound **5** was stable under these conditions. However, prodrugs such as the acetyl ester **10**, isopropyl ester **11**, sodium phosphate ester **15**, and glycine ester **16** all underwent rapid hydrolysis under thermal conditions to give **5**. Aliphatic esters were rapidly hydrolyzed compared to aromatic esters under thermal conditions. Since these esters were not stable under such harsh conditions, they are very likely not suitable for further development as drug candidates. Benzoyl ester **12**, 4-methylbenzoyl ester **13**, pivaloyl ester **14**, 2,6-dimethylbenzoyl ester **18**, and 2,6-dichlorobenzoyl ester **19** were stable under these conditions, and only less than 10% of the compound was hydrolyzed to form **5**. The second criterion for a prodrug is its ability to undergo hydrolysis to release the active drug in the eye. Thus, we selected four compounds (**12**, **14**, **18**, and **19**) that were stable under thermal conditions to study their hydrolysis rates in rabbit eye homogenates. Both 2,6-dimethylbenzoyl ester (**18**) and 2,6-dichlorobenzoyl ester (**19**) were very resistant to hydrolysis, as indicated by very low hydrolysis rates of 1.1 and 1.7 (ng/mL)/h, respectively. Both benzoyl ester **12** and pivaloyl ester **14** underwent hydrolysis at a moderate rate, 288 and 172 (ng/mL)/h, respectively, to generate compound **5**. As anticipated, the aromatic esters with substituents at the ortho positions were resistant to hydrolysis by esterase. The ortho substituents were introduced to modulate the ester hydrolysis by esterases. On

the basis of these favorable properties, compound **12** was selected for further studies.

Since compound **12** was chosen for clinical development on the basis of a combined set of drug substance and drug product properties, we will focus the rest of this article on **12**. Ocular pharmacokinetics using compound **12** were studied in mice, and the data are shown in Table 3. A single drop of 10 μL containing 100 μg (172 nM) of solution of compound **12** was instilled per eye. Both compounds **5** and **12** were detected in the eyes where drops were instilled, suggesting that the prodrug was hydrolyzed to **5**. While the amount of compound **5** seen in the choroid/sclera upon administration of compound **12** reached concentrations similar to that achieved by direct administration of compound **5**, this was not the case in the retina.[43] Much higher levels of **5** were seen in the retina upon topical eye drop administration of **12**. Both compounds **5** and **12** were seen in the choroid and sclera as well as in the retina for more sustained periods of time. The concentrations of **5** and **12** in retina upon instillation of **12** was >30-fold in retina when compared to that of **5** upon direct instillation of **5**. Upon instillation of **12**, the levels of both **5** and **12** reached a maximum in 24 h in the sclera/choroid[44] and in the retina. The conversion of **12** to **5** was observed in both the retina and the sclera/choroids tissue samples. The sustained levels of **5** and **12** in the eye enable us to use a q.d. or q.o.d. dosing schedule. This dosing schedule also showed no eye irritation in the animal models. The plasma concentrations of both **5** and **12** were below the limit of detection (<1 ng/mL) at all time points after topical administration of **12**, suggesting that the compounds are not entering into systemic circulation.[45] The lack of compounds **5** and **12** in systemic circulation is very beneficial, as VEGFr2 inhibitors in systemic circulation are not desirable because of the role VEGFr plays in various biological functions. Therefore, it appears that the administration of compound **12** would enable either once a day or every other day dosing without any systemic buildup of either **5** or **12**.

Possessing a compound with good ocular pharmacokinetics and desirable systemic pharmacokinetics, we turned our efforts to test **12** in a suitable animal model. Choroidal neovascularization (CNV) models in primates,[46] rats,[47] minipigs,[48] and rabbits[49] have been studied extensively. Laser-induced choroidal neovascularization in murine model offers several advantages and has been studied extensively.[50]

After laser-induced rupture of Bruch's membrane at three locations in each eye, mice were treated by topical application t.i.d. with one drop containing 0.61% w/v of **12**, 1.83% w/v of **12**, or vehicle in one eye and no treatment in the fellow eye. A fourth group of mice had rupture of Bruch's membrane and no treatment. After 14 days, eyes that had received drops containing 0.61% w/v (Figure 2A) or 1.83% w/v (Figure 2B) of **12** had CNV lesions that appeared smaller than those in eyes that had received formulation vehicle (Figure 2C) or no treatment (Figure 2D). Measurement of the area of CNV lesions by image analysis showed that compared to the untreated fellow eye, there were statistically significant reductions of 46 ± 7% or 35 ± 9% in the amount of CNV at Bruch's membrane rupture sites in the eyes of mice that were treated with 0.61% w/v or 1.83% w/v of **12**, respectively (Figure 2E). This difference between the treated and fellow eyes indicates that the suppression of CNV occurred by local delivery of **12** and without absorption into the blood stream that could have resulted in systemically mediated drug effects. Relative to vehicle control, there was a reduction of 39 ± 8% or 26 ± 10% in the amount of CNV at Bruch's membrane rupture sites in the eyes of mice that were

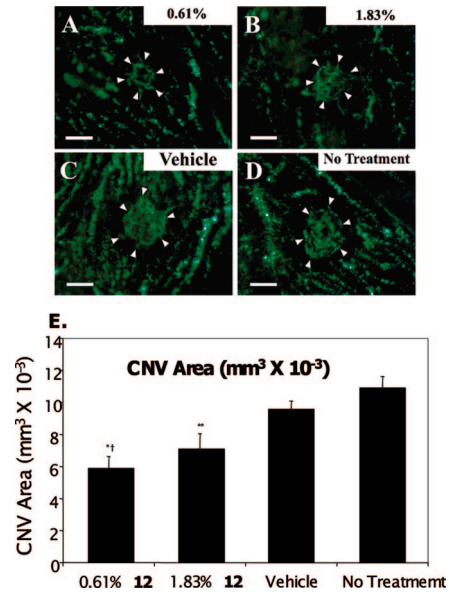

Figure 2. Topical administration of **12** inhibits laser-induced choroidal neovascularization: (A) Representative image of rupture site treated with 0.61% w/v of **12**; (B) representative image of rupture site treated with 1.83% w/v of **12**; (C) representative image of rupture site treated with vehicle; (D) representative image of rupture site untreated; (E) choroidal neovascularization area vs treatment with different concentrations of **12** and controls. Topical administration of **12** reduced laser-induced choroidal neovascularization: 23 eyes/group; (*) $p = 0.0001$, 0.61% **12** vs no treatment; (†) $p = 0.0427$, 0.61% **12** vs vehicle; (**) $p = 0.0063$, 1.83% **12** vs no treatment. The data were analyzed by linear mixed model with the Dunnett method used to adjust for multiple comparisons.

treated with 0.61% or 1.83% **12**, respectively (Figure 2E). There is no statistical difference in biological responses from 0.61% and 1.83% dosing of **12** in the pharmacology model. There was no significant difference between the area of CNV at rupture sites in eyes treated with vehicle and fellow untreated eyes. This demonstrates that the inhibitory effect occurs locally following topical application with no hematogenous delivery to the fellow eye via systemic absorption. These data suggest that topically administered **12** has potential as a noninvasive suppressive therapy for treatment of diseases in which choroidal neovascularization is a significant component of the pathology. Compound **12** was inactive in Src ($IC_{50} \geq 10$ μM), VEGFr2 ($IC_{50} \geq 10$ μM), and YES ($IC_{50} \geq 2.5$ μM) biochemical assays. This would suggest that compound **12** is likely undergoing hydrolysis to release **5** in vivo which is responsible for its biological actions.

The capacity of topically applied **5** or **12** to suppress a VEGF-induced vascular leak in the retina has been demonstrated using a rodent model.[51] In order to establish the molecular target of **5** and its pharmacodynamic effects, the impact of **5** on the phosphorylation of focal adhesion kinase (FAK), a downstream substrate of VEGFr and Src, was studied in eye tissue[52–54] The phosphorylation was monitored in the choroid/sclera of mice undergoing developmental angiogenesis.[55,56] Compound **5** reduced FAK-Y861 phosphorylation in a dose-dependent manner with >90% inhibition observed at the 5 mg/kg dose.[51] The details of the experimental procedure is in the Supporting Information. We have further evaluated the efficacy of compounds **5** and **12** in VEGF induced retinal leak model. As mentioned before, VEGF-induced vascular leakage is a significant pathology contributing to vision loss in AMD, PDR, and DME. On the basis of these attributes, the capacity of topically

applied **5** or **12** to suppress a VEGF-induced vascular leak in the retina was assessed in a rodent model. Briefly, VEGF was injected and vitreous plasma leak was monitored at the back of the eye. Compounds **5** (0.7% w/v) and **12** (1.22% w/v) were instilled topically in a suitable media. Compound **5** decreased VEGF-induced leak by 60% after single topical instillation, q.d., to a mice model of VEGF induced retinal leak. When the compound **5** was administered t.i.d., there was a 80% decrease in VEGF induced leak response. However, a topical administration of **12**, q.d., completely abolished VEGF-induced leak in the above animal model. The prodrug **12** not only showed increased efficacy but also reduced frequency of administration. The details of VEGF induced leak model and the effects of compounds **5** and **12** on the model are in the Supporting Information.

Conclusions

We have developed a series of benzotriazine-based compounds that inhibit Src and VEGFr2, both of which play critical roles in age-related macular degeneration. We optimized the inhibitory activity of a series of benzotriazine compounds toward both Src and VEGFr2. On the basis of in vitro activity in enzymatic and cellular assays, compound **5** was selected and studied further in ocular PK studies. However, compound **5** showed lower than expected ocular pharmacokinetic properties because of its inability to attain sustained concentrations in certain back-of-the-eye tissue. Subsequently, several prodrugs of **5** were prepared and evaluated for their thermal stability at higher temperature to identify appropriate prodrugs that are suitable for further development. Prodrugs that were stable under thermal conditions were selected and their hydrolysis rates in ocular tissue were evaluated as a surrogate for their propensity to generate the active compound **5** in the in vivo setting. Prodrug **12** showed much better pharmacokinetic properties compared to **5** and released sufficient amounts of **5** over sustained periods of time in the choroid, sclera, and retina. The analysis of blood samples withdrawn over time, after topical delivery of **12** as an eye drop, revealed that the amount of **12** or **5** in the systemic circulation was below quantifiable limits.

In order to evaluate the capacity of **5** to inhibit choroidal angiogenesis, prodrug **12** was tested in a model of choroidal angiogenesis in which angiogenesis is caused using laser-induced rupture of Bruch's membrane in the eyes of C57BL/6 mice. After laser-induced rupture of Bruch's membrane, mice were treated by topical application with **12**. Relative to vehicle control, there is a reduction of 39 ± 8% and 26 ± 10% in the amount of CNV at Bruch's membrane rupture sites in the eyes of mice treated with 0.61% w/v and 1.83% w/v of **12**, respectively.

Because of its in vitro activity in enzymatic and cellular assays, **5** was selected for the prodrug approach to improve its pharmacokinetic properties. On the basis of its favorable ocular pharmacokinetics and activity in a preclinical model, compound **12** was selected for further development for age-related macular degeneration. Compound **12** is currently undergoing evaluation in clinical trials for age-related macular degeneration.[57,58]

Experimental Section

All experiments were performed under anhydrous conditions in an atmosphere of argon, except where stated, using oven-dried apparatus and employing standard techniques in handling air-sensitive materials. All the solvents and chemicals from commercial sources were used as received without further purification. Aqueous solutions of sodium bicarbonate and sodium chloride (brine) were saturated. Analytical thin layer chromatography (TLC) was carried out using Merck Kieselgel 60 F_{254} plates with visualization by ultraviolet and/or anisaldehyde, potassium permanganate, or phosphomolybdic acid dips. Flash chromatography was carried out using RediSep 45–60 μm silica gel columns using the Isco CombiFlash companion system. Preparative reverse-phase HPLC chromatography was carried out on Gilson preparative HPLC equipped with a 215 liquid handler and Waters SymmetryShield TM RP18 7μm (40 mm × 100 mm) Prep-Pak cartridge. The mobile phase consisted of HPLC grade acetonitrile and water, both containing 0.1% trifluoroacetic acid. Purification was carried out at a flow rate of 40 mL/min and a gradient such that the peak of interest was eluted between 12 and 15 min in a 30 min run. ^{1}H NMR spectra were recorded at NuMega Laboratories (San Diego, CA) on a Bruker AMX-II spectrometer operating at 500 MHz. Spectra were obtained on all the intermediates and the final products in deuterated dimethyl sulfoxide (DMSO-d_6) unless otherwise noted and were consistent with the proposed structures. Chemical shifts are calibrated to tetramethylsilane internal standard or residual solvent peak and expressed in δ (ppm) units. Peak multiplicities are represented as follows: s = singlet, d = doublet, t = triplet, q = quartet, qn = quintet, dd = doublet of doublets, m = multiplet, br s = broad singlet). Coupling constants (J/Hz) and integration are also listed. Coupling constants were taken directly from the spectra and are uncorrected. Mass spectrometry was carried out on a Waters analytical LC−MS system equipped with a C-18 reverse phase column. The analytical gradient consisted of 10% acetonitrile in water ramping up to 100% acetonitrile, both containing 0.05% trifluoroacetic acid, over 5 min unless otherwise stated. Low-resolution mass spectra was obtained on a micromass spectrometer using the electrospray (ES+) ionization method. The protonated parent ion (M + 1) or fragment of highest mass was quoted. The mass spectral data were consistent with the proposed structure. Purities of compounds were measured on a Shimadzu HPLC equipped with a Agilent C-18 Zorbax 250 mm × 4.6 mm column with 5 μm particle size and dual wavelength and evaporating light scattering detectors (ELSD). The analytical gradient consisted of 10% acetonitrile in water ramping up to 100% acetonitrile, both containing 0.05% trifluoroacetic acid, over 20 min unless otherwise stated. The column temperature was maintained at 40 °C for all the purity analyses. Elemental analyses were performed at NuMega Laboratories (San Diego, CA) on Perkin-Elmer series II-2400 CHNS analyzer, and the results are within 0.4% of the calculated values unless otherwise stated.

7-Phenyl-5-methyl-*N*-[4-(2-pyrrolidin-1-ylethoxy)phenyl]-1,2,4-benzotriazin-3-amine (1). The title compound was prepared using the procedure that is described for compound **26c** and converted to the hydrochloride salt using dioxane−hydrogen chloride solution (35%). ^{1}H NMR: δ 1.80–2.10 (m, 4H), 2.68 (s, 3H), 3.05–3.15 (m, 2H), 3.55–3.65 (m, 4H), 4.37 (t, J = 5.1 Hz, 2H), 7.09 (d, J = 9.1 Hz, 2H), 7.44 (t, J = 7.6 Hz, 1H), 7.54 (t, J = 7.6 Hz, 2H), 7.88 (d, J = 7.6 Hz, 2H), 7.98 (d, J = 9.0 Hz, 2H), 8.17 (s, 1H), 8.40 (d, J = 1.7 Hz, 1H), 10.83 (s, 2H). MS-ESI$^+$ m/z 426 [M + 1]. Anal. ($C_{26}H_{27}N_5O\cdot HCl\cdot 0.5H_2O$) C, H, N. HPLC purity, 97% at 220 nm.

7-(2-Chlorophenyl)-5-methyl-*N*-[4-(2-pyrrolidin-1-ylethoxy)phenyl]-1,2,4-benzotriazin-3-amine (2). The title compound was prepared using the procedure that is described for compound **26c** and converted to the hydrochloride salt using dioxane−hydrogen chloride solution (38%). ^{1}H NMR: δ 1.85–2.05 (m, 4H), 2.65 (s, 3H), 3.05–3.15 (m, 2H), 3.55–3.65 (m, 4H), 4.36 (t, J = 5.0 Hz, 2H), 7.09 (d, J = 9.2 Hz, 2H), 7.40–7.55 (m, 2H), 7.55–7.65 (m, 2H), 7.86 (dd, J = 0.95, 1.8 Hz, 1H), 7.98 (d, J = 9.1 Hz, 2H), 8.17 (d, J = 1.8 Hz, 1H), 10.70 (br s, 1H), 10.89 (br s, 1H). MS-ESI$^+$ m/z 460 [M + 1]. Anal. ($C_{26}H_{26}ClN_5O\cdot HCl\cdot 0.5H_2O$) C, H, N. HPLC purity 97% at 220 nm.

7-(2,6-Dimethylphenyl)-5-methyl-*N*-[4-(2-pyrrolidin-1-ylethoxy)phenyl]-1,2,4-benzotriazin-3-amine (3). A solution of 7-(2,6-dimethylphenyl)-5-methylbenzo[1,2,4]triazin-3-ylamine (1 g, 3.78 mmol) and of 1-[2-(4-bromophenoxy)ethyl]pyrrolidine (2.04 g, 7.56 mmol), tris(dibenzylideneacetone)dipalladium(0) (174 mg, 0.19 mmol), (±)-2,2′-bis(diphenylphosphino)-1,1′-binaphthalene (340 mg, 0.54 mmol),

and potassium *tert*-butoxide (500 mg, 4.46 mmol) in toluene (500 mL) under argon was heated at 100 °C for 24 h. The reaction mixture was concentrated under reduced pressure, dissolved in dimethyl formamide, and purified by preparative HPLC to afford the title compound (0.09 g, 5.2%). ^{1}H NMR: δ 1.90–2.05 (m, 10 H), 2.64 (s, 3H), 3.14–3.16 (m, 2H), 3.59–3.64 (m, 4H), 4.31 (t, J = 5.2 Hz, 2H), 7.09 (d, J = 9.2 Hz, 2H), 7.18 (d, J = 7.4 Hz, 2H), 7.22–7.24 (m, 1H), 7.60 (s, 1H), 7.91 (s, 1H), 7.98 (d, J = 9.2 Hz, 2H). MS-ESI$^+$ m/z 454 [M + 1]. Anal. ($C_{28}H_{31}N_5O \cdot C_6H_8O_7 \cdot 1.5H_2O$) C, H, N. HPLC purity 99% at 220 nm.

7-(2,6-Dichlorophenyl)-5-methyl-*N*-[4-(2-pyrrolidin-1-ylethoxy)-phenyl]-1,2,4-benzotriazin-3-amine (4). The title compound was synthesized using a similar procedure described for **3** to afford the title compound (35%). ^{1}H NMR: δ 1.88–1.91 (m, 2H), 2.02–2.07 (m, 2H), 2.63 (s, 3H), 3.12–3.17 (m, 2H), 3.58–3.62 (m, 4H), 4.32 (t, J = 4.8 Hz, 2 H), 7.10 (d, J = 9.2 Hz, 2H), 7.51 (t, J = 8.2 Hz, 1H), 7.67 (d, J = 8.2 Hz, 2H), 7.69 (dd, J = 1.0, 1.9 Hz, 1H), 7.98 (d, J = 9.2 Hz, 2H), 8.08 (s, 1H). MS-ESI$^+$ m/z 494 (M + 1). Anal. ($C_{26}H_{25}Cl_2N_5O \cdot 0.5H_2O$) C, H, N. HPLC 99% pure at 230 nM and 100% pure using ELSD detector.

General Procedure for the Deprotection of a Methoxy Group with Boron Tribromide (BBr_3). A solution of methoxy precursor (1.0 mol equiv) and boron tribromide (5–10 mol equiv) in dichloromethane (0.01–0.03 M) was stirred at room temperature until the reaction was complete (4–12 h). The pH of the reaction mixture was adjusted to 7 by treating with a saturated sodium bicarbonate solution and filtered. The solids were washed with water and ether and purified using preparative HPLC to afford pure compounds.

4-Chloro-3-(5-methyl-3-{[4-(2-pyrrolidin-1-ylethoxy)phenyl]amino}-1,2,4-benzotriazin-7-yl)phenol (5). The methoxy group in 7-(2-chloro-5-methoxyphenyl)-5-methyl-*N*-[4-(2-pyrrolidin-1-ylethoxy)phenyl]-1,2,4-benzotriazin-3-amine (**26a**, 440 mg, 0.90 mmol) was cleaved using boron tribromide as described in the general procedure to afford the title compound (387 mg, 84%), which was converted to the HCl salt. ^{1} H NMR: δ 1.88–1.92 (m, 2H), 1.97–2.05 (m, 2H), 2.64 (s, 3H), 3.09–3.14 (m, 2H), 3.57–3.61 (m, 4H), 4.36 (t, J = 4.9 Hz, 2H), 6.87 (dd, J = 2.9, 8.8 Hz, 1H), 6.94 (d, J = 2.9 Hz, 1H), 7.09 (d, J = 9.0 Hz, 2H), 7.39 (d, J = 8.8 Hz, 1H), 7.83 (d, J = 1.6 Hz, 1H), 7.98 (d, J = 9.0 Hz, 2H), 8.12 (d, J = 1.6 Hz, 1H), 9.97 (s, 1H), 10.55 (br s, 1H), 10.87 (s, 1H). MS-ESI$^+$ m/z 476 (M + 1). Anal. ($C_{26}H_{26}ClN_5O_2 \cdot HCl \cdot 0.25H_2O$) C, H, N. HPLC 98% pure at 220 nm, 98% pure using ELSD detector.

4-{[7-(2-Chloro-5-hydroxyphenyl)-5-methyl-1,2,4-benzotriazin-3-yl]amino}-*N*-(2-pyrrolidin-1-ylethyl)benzenesulfonamide (6). The methoxy group in 4-{[7-(2-chloro-5-methoxyphenyl)-5-methyl-1,2,4-benzotriazin-3-yl]amino}-*N*-(2-pyrrolidin-1-ylethyl)benzene-sulfonamide (**26b** 0.055 g, 0.099 mmol) was cleaved using boron tribromide as described in the general procedure to afford the title compound as the trifluoroacetate salt (0.013 g, 25% yield). ^{1}H NMR: δ 1.85–1.88 (m, 2H), 1.95–1.99 (m, 2H), 2.98–3.03 (m, 2H), 3.10–3.14 (m, 2H), 3.21–3.25 (m, 2H), 3.38 (s, 3H), 3.50–3.54 (m, 2H), 6.89 (dd, J = 2.9, 8.7 Hz, 1H), 6.96 (d, J = 2.9 Hz, 1H), 7.41 (d, J = 8.7 Hz, 1H), 7.88 (d, J = 8.9 Hz, 2H), 7.92 (d, J = 1.8 Hz, 1H), 8.21 (d, J = 1.7 Hz, 1H), 8.25 (d, J = 8.8 Hz, 2H), 10.00 (s, 1H), 10.43 (br s, 1H) 11.44 (s, 1H). MS-ESI$^+$ m/z 539 (M + 1). Anal. ($C_{26}H_{27}ClN_6O_3S \cdot HCl \cdot H_2O$) C, H, N. HPLC 97% pure at 220 nm and at 254 nm.

4-Chloro-3-(5-methyl-3-{[4-(piperazin-1-ylcarbonyl)phenyl]amino}-1,2,4-benzotriazin-7-yl)phenol (7). The title compound, was prepared from *tert*-butyl 4-(4-{[7-(2-chloro-5-methoxyphenyl)-5-methyl-1,2,4-benzotriazin-3-yl]amino}benzoyl)piperazine-1-carboxylate (**26c**, 40 mg, 0.068 mmol) as described in the general procedure using boron tribromide. Both methyl groups and the *tert*-butyloxycarbonyl group in **26c** were cleaved simultaneously under the reaction conditions, and the crude product was purified by preparative HPLC to afford the title compound as an orange solid (32 mg, 99% yield). ^{1}H NMR: δ 2.69 (s, 3H), 2.70–2.80 (m, 4H), 3.35–3.50 (m, 4H), 6.87 (dd, J = 2.9, 8.7 Hz, 1H), 6.94 (d, J = 2.9 Hz, 1H), 7.41 (d, J = 8.7 Hz, 1H), 7.46 (d, J = 8.7 Hz, 2H), 7.85–7.90 (m, 1H), 8.09 (d, J = 8.6 Hz, 2H), 8.18 (d, J = 1.7 Hz, 1H), 9.93 (br s, 1H), 11.17 (s, 1H). MS-ESI$^+$ m/z 475 (M + 1). Anal. ($C_{25}H_{23}ClN_6O_2 \cdot 2H_2O$) C, H, N.

7-(2-Chloro-5-hydroxyphenyl)-5-methyl-*N*-[4-(piperidin-4-ylsulfonyl)phenyl]-1,2,4-benzotriazin-3-amine (8). The methoxy group and benzyl carboxylate in benzyl 4-[(4-{[7-(2-chloro-5-methoxyphenyl)-5-methyl-1,2-4-benzotriazin-3-yl]amino}phenyl)sulfonyl]piperdine-1-carboxylate (**26d**, 0.165 g, 0.25 mmol) were cleaved using boron tribromide in dichloromethane (2.5 mL, 2.5 mmol) as described in the general procedure to afford the title compound as a yellow solid (0.028 g, 22%). ^{1}H NMR: δ 1.68–1.77 (m, 2H), 2.03–2.06 (m, 2H), 2.73 (s, 3H), 2.83–2.88 (m, 2H), 3.05 (s, 1H), 3.52–3.58 (m, 1H), 6.89 (dd, J = 2.9, 8.8 Hz, 1H), 6.95 (d, J = 2.9 Hz, 1H), 7.41 (d, J = 8.7 Hz, 1H), 7.88 (d, J = 8.8 Hz, 2H), 7.94 (s, 1H), 8.23 (d, J = 1.7 Hz, 1H), 8.33 (d, J = 8.8 Hz, 2H), 8.75 (br s, 1H), 10.00 (s, 1H), 11.57 (s, 1H). MS-ESI$^+$ m/z 510 (M + 1). Anal. ($C_{25}H_{24}ClN_5O_3S \cdot C_2F_3HO_2 \cdot 1.2H_2O$) C, H, N.

7-(2-Chloro-5-hydroxyphenyl)-5-methyl-*N*-[4-(3-pyrrolidin-1-ylpropyl)]phenyl]-1,2,4-benzotriazin-3-amine (9). A suspension of [7-(2-chloro-5-methoxyphenyl)-5-methyl]-1,2,4-benzotriazin-3-amine (0.55 g, 1.8 mmol), 1-[3-(4-bromophenyl)propyl]pyrrolidine (0.60 g, 2.2 mmol), palladium acetate (25 mg, 0.11 mmol), xantphos (0.13 g, 0.22 mmol), and potassium *tert*-butoxide (0.40 g, 3.6 mmol) in dioxane (3 mL) was heated at reflux for 16 h. The reaction mixture was cooled to room temperature and filtered, and the solids were washed with dichloromethane. The filtrate was concentrated under reduced pressure and purified by flash chromatography (SiO_2, 10–20% methanol in dichloromehtane) to afford 7-(2-chloro-5-methoxyphenyl)-5-methyl-*N*-[4-(3-pyrrolidin-1-ylpropyl)]phenyl]-1,2,4-benzotriazin-3-amine as a red solid (0.16 g, 18%). MS (ESI+): m/z 488 $(M + 1)^+$. This compound (0.16 g, 0.33 mmol) was treated with boron tribromide as described in the general procedure to cleave the methyl group. The reaction mixture was purified by preparative HPLC to afford the title compound as an orange solid (30 mg, 16%). ^{1}H NMR: δ 1.80–1.90 (m, 2H), 1.90–2.05 (m, 4H), 2.64 (t, J = 7.6 Hz, 2H), 2.66 (s, 3H), 2.95–3.05 (m, 2H), 3.10–3.20 (m, 2H), 3.50–3.70 (m, 2H), 6.87 (dd, J = 2.9, 8.8 Hz, 1H), 6.93 (d, J = 2.9 Hz, 1H), 7.28 (d, J = 8.5 Hz, 2H), 7.40 (d, J = 8.8 Hz, 1H), 7.85 (t, J = 0.8 Hz, 1H), 7.98 (d, J = 8.5 Hz, 2H), 8.15 (d, J = 1.8 Hz, 1H), 9.55 (br s, 1H), 9.95 (br s, 1H), 10.94 (s, 1H). MS-ESI$^+$ m/z 474 (M + 1). Anal. ($C_{27}H_{28}ClN_5O \cdot C_2F_3HO_2 \cdot 1.5H_2O$) C, H, N.

4-Chloro-3-(5-methyl-3-{[4-(2-pyrrolidin-1-ylethoxy)phenyl]amino}-1,2,4-benzotriazin-7-yl)phenyl Acetate (10). Acetyl chloride (0.092 g, 1.17 mmol) was added dropwise to a solution of 4-chloro-3-(5-methyl-3-{[4-(2-pyrrolidin-1-ylethoxy)phenyl]amino}-1,2,4-benzotriazin-7-yl)phenol hydrochloride (**5**, 0.465 g, 0.978 mmol) and triethylamine (0.494 g, 4.89 mmol) in dichloromethane (30 mL) under argon at room temperature and stirred for 24 h. The reaction mixture was quenched with a saturated sodium bicarbonate solution. The organic layer was separated, dried (Na_2SO_4), filtered, concentrated under reduced pressure, and purified on flash chromatography (SiO_2, dichloromethane/methanol/triethylamine = 85:10:5 (v/v/v)) to afford the title compound as an orange solid (0.409 g, 75%). ^{1}H NMR: δ 1.67–1.70 (m, 4H), 2.29 (s, 3H), 2.50–2.52 (m, 4H), 2.64 (s, 3H), 2.78 (t, J = 5.9 Hz, 2H), 4.07 (t, J = 6.0 Hz, 2H), 6.99 (dd, J = 7.1, 12.6 Hz, 2H), 7.27 (dd, J = 5.9, 8.8 Hz, 1H), 7.41 (d, J = 2.8 Hz, 1H), 7.67 (d, J = 8.8 Hz, 1H), 7.85 (t, J = 1.3 Hz, 1H), 7.93 (d, J = 9.1 Hz, 2H), 8.17 (d, J = 1.8 Hz, 1H), 10.83 (s, 1H). MS-ESI$^+$ m/z 520 (M + 3). Anal. ($C_{28}H_{28}ClN_5O_3 \cdot 0.5H_2O$) C, H, N.

4-Chloro-3-(5-methyl-3-{[4-(2-pyrrolidin-1-ylethoxy)phenyl]amino}-1,2,4-benzotriazin-7-yl)-4-phenyl 2-Methylpropanoate (11). The title compound was prepared using a procedure similar to that described for **10**. Compound **11** was obtained in comparable yield. ^{1}H NMR: δ 1.24 (d, J = 6.9 Hz, 6H), 1.67–1.71 (m, 4H), 2.52–2.54 (m, 4H), 2.64 (s, 3H), 2.79 (t, J = 5.9 Hz, 2H), 4.07 (t, J = 5.9 Hz, 2H), 6.99 (d, J = 7.1 Hz, 2H), 7.25 (dd, J = 2.9, 8.8 Hz, 1H), 7.41 (d, J = 2.9 Hz, 1H), 7.67 (d, J = 8.8 Hz, 1H), 7.85 (t, J = 1.1 Hz, 1H), 7.93 (d, J = 9.1 Hz, 2H), 8.18 (d, J = 1.9 Hz, 1H), 10.84 (s, 1H). MS-ESI$^+$ m/z 546 (M + 1). HPLC purity, 95% at 254 nm.

4-Chloro-3-(5-methyl-3-{[4-(2-pyrrolidin-1-ylethoxy)phenyl]amino}-1,2,4-benzotriazin-7-yl)phenyl Benzoate (12). The title compound was synthesized from 4-chloro-3-(5-methyl-3-{[4-(2-pyrrolidin-1-ylethoxy)phenyl]amino}-1,2,4-benzotriazin-7-yl)phenol hydrochloride (**5**, 1.0 g, 2.0 mmol) as described for compound **10** (0.9 g, 80%). ^{1}H NMR: δ 1.65–1.72 (m, 4H), 2.50–2.56 (m, 4H), 2.63 (s, 3H), 2.79 (t, J = 5.9 Hz, 2H), 4.07 (t, J = 6.0 Hz, 2H), 7.00 (d, J = 9.1 Hz, 2H), 7.46 (dd, J = 2.9, 8.7 Hz, 1H), 7.60–7.65 (m, 3H), 7.75 (d, J = 8.6 Hz, 1H), 7.76 (t, J = 7.4 Hz, 1H), 7.90 (dd, J = 1.0, 1.8 Hz, 1H), 7.93 (d, J = 9.1 Hz, 2H), 8.16 (d, J = 8.4 Hz, 2H), 8.22 (d, J = 1.8 Hz, 1H), 10.84 (br s, 1H). MS-ESI$^+$ m/z 580 (M + 1). Anal. ($C_{33}H_{30}ClN_5O_3 \cdot HCl \cdot 0.5H_2O$) C, H, N. HPLC 98% pure at 220 nm and 100% pure using ELSD detector.

4-Chloro-3-(5-methyl-3-{[4-(2-pyrrolidin-1-ylethoxy)phenyl]amino}-1,2,4-benzotriazin-7-yl)phenyl 4-Methylbenzoate (13). The title compound was prepared similar to the procedure described for **10**. ^{1}H NMR: δ 1.68–1.70 (m, 4H), 2.42 (s, 3H), 2.51–2.53 (m, 4H), 2.64 (s, 3H), 2.78 (t, J = 6.0 Hz, 2H), 4.06 (t, J = 6.0 Hz, 2H), 6.99 (d, J = 5.0 Hz, 2H), 7.42 (d, J = 7.5 Hz, 2H), 7.44 (d, J = 2.8 Hz, 1H), 7.58 (d, J = 2.8 Hz, 1H), 7.72 (d, J = 8.7 Hz, 1H), 7.88 (d, J = 0.9 Hz, 1H), 7.92 (d, J = 9.2 Hz, 2H), 8.05 (d, J = 6.6 Hz, 2H), 8.21 (d, J = 1.8 Hz, 1H), 10.83 (s, 1H). MS-ESI$^+$ m/z 594 (M + 1). HPLC purity, 98% at 254 nm.

4-Chloro-3-(5-methyl-3-{[4-(2-pyrrolidin-1-ylethoxy)phenyl]amino}-1,2,4-benzotriazin-7-yl)phenyl Pivalate (14). A solution of 4-chloro-3-{5-methyl-3-[4-(2-pyrrolidin-1-ylethoxy)phenylamino]benzo[1,2,4]triazin-7-yl}phenol hydrochloride (**5**, 1.86 g, 3.91 mmol), triethylamine (3.95 g, 39.1 mmol) in dichloromethane (100 mL) under argon atmosphere was stirred for 10 min. Pivoloyl chloride (0.616 g, 5.09 mmol) was added dropwise to the solution and stirred at room temperature for 2 h. A solution of saturated sodium bicarbonate (25 mL) was added, and the organic layer was separated, dried (Na_2SO_4), filtered, concentrated under reduced pressure, and purified using preparative HPLC to afford the title compound (2.14 g, 98% yield). ^{1}H NMR: δ 1.31 (s, 9H), 1.67–1.69 (m, 4H), 2.51–2.53 (m, 4H), 2.64 (s, 3H), 2.80 (t, J = 5.7 Hz, 2H), 4.07 (t, J = 5.9 Hz, 2H), 7.00 (d, J = 7.1 Hz, 2H), 7.24 (dd, J = 5.9, 8.8 Hz, 1H), 7.39 (d, J = 2.8 Hz, 1H), 7.67 (d, J = 8.7 Hz, 1H), 7.85 (s, 1H), 7.92 (d, J = 9.1 Hz, 2H), 8.18 (d, J = 1.8 Hz, 1H). MS-ESI$^+$ m/z 560 (M + 1). Anal. ($C_{31}H_{34}ClN_5O_3$) C, H, N. HPLC 99% pure at 220 nm and 99% pure using ELSD.

Disodium 4-Chloro-3-(5-methyl-3-{[4-(2-pyrrolidin-1-yl-ethoxy)phenyl]amino}-1,2,4-benzotriazin-7-yl)phenyl Phosphate (15). A solution of 4-chloro-3-{5-methyl-3-[4-(2-pyrrolidin-1-ylethoxy)-phenylamino]benzo[1,2,4]triazin-7-yl}phenol (**5**, 0.51 g, 1.0 mmol), phosphorus oxychloride (0.46 g, 3.0 mmol), and triethylamine (1.0 g, 10 mmol) in dichloromethane (100 mL) was stirred at room temperature for 12 h. An aqueous sodium bicarbonate solution (0.5 g in 6 mL of water) was added to the reaction mixture and stirred at room temperature for 30 min. The organic layer was separated, dried (Na_2SO_4), filtered, and concentrated and the solid was washed with water (20 mL), methanol (20 mL), and ether (20 mL) to afford the title compound as a red solid (430 mg, 72%). ^{1}H NMR: δ 1.86–1.88 (m, 4H), 2.88–3.01 (m, 4H), 3.17 (s, 3H), 3.34 (br s, 2H), 4.14–4.18 (m, 2H), 6.90 (d, J = 8.9 Hz, 2H), 7.21 (dd, J = 2.8, 8.9 Hz, 1H), 7.31 (s, 1H), 7.43 (d, J = 8.8 Hz, 1H), 7.70 (s, 1H), 7.78 (d, J = 8.9 Hz, 2H), 7.96 (s, 1H), 10.65 (s, 1H). MS-ESI$^+$ m/z 556 (M + 1). Anal. ($C_{26}H_{25}ClN_5Na_2O_5P \cdot H_2O$) C, H, N. HPLC purity >98% at 220 nm.

4-Chloro-3-(5-methyl-3-{[4-(2-pyrrolidin-1-ylethoxy)phenyl]amino}-1,2,4-benzotriazin-7-yl)phenyl Glycinate (16). 4-Chloro-3-(5-methyl-3-{[4-(2-pyrrolidin-1-ylethoxy)phenyl]amino}-1,2,4-benzotriazin-7-yl)phenyl(*N*-butyloxycarbonyl) glycinate (**28**, 0.012 g, 0.019 mmol) was stirred in a 5% solution of trifluoroacetic acid in dichloromethane for 1 h at room temperature. The reaction mixture was concentrated and purified on preparative HPLC to afford the title compound as the trifluoroacetate salt (0.008 g, 80%). ^{1}H NMR: δ 1.80–2.10 (m, 4H), 2.64 (s, 3H), 3.10–3.20 (m, 2H), 3.55–3.65 (m, 4H), 4.15 (br s, 2H), 4.31 (t, J = 5.3 Hz, 2H), 7.10 (d, J = 9.2 Hz, 2H), 7.34 (dd, J = 2.9, 8.7 Hz, 1H), 7.46 (d, J = 2.8 Hz, 1H), 7.7 (d, J = 8.7 Hz, 1H), 7.88 (dd, J = 1.4, 1.9 Hz, 1H), 7.98 (d, J = 9.1 Hz, 2H), 8.20 (d, J = 1.8 Hz, 1H), 8.46 (br s, 2H), 9.87 (br s, 1H), 10.92 (br s, 1H). MS-ESI$^+$ m/z 533 (M + 1)$^+$. HPLC purity, 97% at 254 nm.

4-Chloro-3-(5-methyl-3-{[4-(2-pyrrolidin-1-ylethoxy)phenyl]amino}-1,2,4-benzotriazin-7-yl)phenyl Nicotinate (17). A solution of 4-chloro-3-(5-methyl-3-{[4-(2-pyrrolidin-1-ylethoxy)phenyl]amino}-1,2,4-benzotriazin-7-yl)phenol (**5**, 320 mg, 0.63 mmol), nicotinyl chloride (122 mg, 0.69 mmol), and triethylamine (0.64 g, 6.3 mmol) in dichloromethane (50 mL) was stirred at room temperature for 12 h. A saturated aqueous sodium bicarbonate solution (100 mL) was added to the reaction mixture, and the organic layer was separated. The aqueous layer was extracted with dichloromethane (2 × 20 mL). The organic layers were combined, washed with brine (100 mL), and dried (Na_2SO_4). The solvent was removed under reduced pressure and the solid was washed with ether (2 × 30 mL) to afford the title compound as a red solid (177 mg, 49%). ^{1}H NMR: δ 1.65–1.75 (m, 4H), 2.57 (br s, 4H), 2.65 (s, 3H), 2.83 (br s, 2H), 4.09 (t, J = 5.9 Hz, 2H), 7.00 (d, J = 9.1 Hz, 2H), 7.50 (dd, J = 2.8, 8.7 Hz, 1H), 7.55–7.68 (m, 2H), 7.76 (d, J = 8.7 Hz, 1H), 7.90 (s, 1H), 7.93 (d, J = 9.1 Hz, 2H), 8.22 (s, 1H), 8.40–8.50 (m, 1H), 8.91 (dd, J = 1.7, 4.8 Hz, 1H), 9.28 (d, J = 2.3 Hz, 1H), 10.84 (s, 1H). MS-ESI$^+$ m/z 581 (M + 1). HPLC purity, 98% at 254 nm.

4-Chloro-3-(5-methyl-3-{[4-(2-pyrrolidin-1-ylethoxy)phenyl]amino}-1,2,4-benzotriazin-7-yl)phenyl 4-(2,6-Dimethylbenzoate) (18). A solution of 4-chloro-3-(5-methyl-3-{[4-(2-pyrrolidin-1-ylethoxy)-phenyl]amino}-1,2,4-benzotriazin-7-yl)phenol (**5**, 0.39 g, 0.768 mmol), 2,6-dimethylbenzoyl chloride (0.168 g, 0.998 mmol), and triethylamine (1.6 mL, 11.5 mmol) in dichloromethane (20 mL) was stirred under argon atmosphere at room temperature for 12 h. The reaction mixture was washed with saturated aqueous sodium bicarbonate solution (20 mL), dried (Na_2SO_4), filtered, concentrated under reduced pressure, and purified using flash chromatography (SiO_2, 10% methanol in dichloromethane) to afford the title compound as a red solid (0.10 g, 21%). ^{1}H NMR: δ 1.65–1.75 (m, 4H), 2.35–2.45 (m, 6H), 2.55–2.60 (m, 4H), 2.66 (s, 3H), 2.80–2.90 (br s, 2H), 4.09 (t, J = 5.9 Hz, 2H), 7.01 (d, J = 9.2 Hz, 2H), 7.19 (d, J = 7.6 Hz, 2H), 7.34 (t, J = 7.7 Hz, 1H), 7.47 (dd, J = 3.0, 8.8 Hz, 1H), 7.59 (d, J = 2.8 Hz, 1H), 7.77 (d, J = 8.8 Hz, 1H), 7.90–8.01 (m, 3H), 8.23 (d, J = 1.8 Hz, 1H), 10.86 (s, 1H). MS-ESI$^+$ m/z 609 (M + 1)$^+$. HPLC purity 95% using ELSD.

4-Chloro-3-(5-methyl-3-{[4-(2-pyrrolidin-1-ylethoxy)phenyl]amino}-1,2,4-benzotriazin-7-yl)phenyl 4-(2,6-Dichlorobenzoate) (19). A solution of 4-chloro-3-(5-methyl-3-{[4-(2-pyrrolidin-1-ylethoxy)-phenyl]amino}-1,2,4-benzotriazin-7-yl)phenol (**5** 0.25 g, 0.53 mmol), 2,6-dichlorobenzoyl chloride (0.144 g, 0.69 mmol), and triethylamine (0.074 mL, 5.3 mmol) in dichloromethane (5 mL) was stirred under argon atmosphere at room temperature for 24 h. The reaction mixture was concentrated under reduced pressure and purified using flash chromatography (SiO_2, 10% methanol in dichloromethane) to afford the title compound as a red solid (0.30 g, 94%). ^{1}H NMR: δ 1.55–1.65 (m, 4H), 2.52–2.58 (m, 4H), 2.65 (s, 3H), 2.75–2.85 (m, 2H), 4.08 (t, J = 5.9 Hz, 2H), 7.01 (dd, J = 2.0, 7.1 Hz, 2H), 7.45 (d, J = 11.4 Hz, 1H), 7.51 (d, J = 2.8 Hz, 1H), 7.60–7.65 (m, 1H), 7.69 (s, 1H), 7.71 (d, J = 1.6 Hz, 1H), 7.81 (d, J = 8.8 Hz, 1H), 7.89 (dd, J = 0.9, 1.8 Hz, 1H), 7.94 (d, J = 9.1 Hz, 2H), 8.23 (d, J = 1.8 Hz, 1H), 10.86 (br s, 1H). MS-ESI$^+$ m/z 650 (M + 3). HPLC purity, 98% at 254 nm.

4-Chloro-3-(5-methyl-3-{[4-(2-pyrrolidin-1-ylethoxy)phenyl]amino}-1,2,4-benzotriazin-7-yl)phenyl 4-(Morpholin-4-ylmethyl)benzoate (20). A solution of 4-chloro-3-(5-methyl-3-{[4-(2-pyrrolidin-1-ylethoxy)phenyl]amino}-1,2,4-benzotriazin-7-yl)phenol (**5**, 0.77 g, 1.5 mmol), 4-(morpholinomethyl)benzoic acid (1.06 g, 4.8 mmol), *N*-(3-dimethylaminopropyl)-*N*′-ethylcarbodiimide hydrochloride (2.36 g, 12.31 mmol), and 4-dimethylaminopyridine (0.225 g, 1.85 mmol) in dimethylformamide (60 mL) was stirred under argon atmosphere at room temperature for 12 h. The reaction mixture was concentrated, suspended in dichloromethane, and washed with saturated sodium bicarbonate solution and brine. The organic layer was dried (Na_2SO_4), filtered, concentrated under reduced pressure, and purified

(SiO_2, 10% methanol in dichloromethane) to afford the title compound (1.29 g, 97%). ^{1}H NMR: δ 1.60–1.75 (m, 4H), 2.30–2.40 (m, 4H), 2.50–2.60 (m, 4H), 2.64 (s, 3H), 2.80 (t, J = 5.8 Hz, 2H), 3.50–3.65 (m, 6H), 4.08 (t, J = 5.8 Hz, 2H), 7.00 (d, J = 9.1 Hz, 2H), 7.43 (dd, J = 2.9, 8.8 Hz, 1H), 7.55 (d, J = 8.5 Hz, 2H), 7.59 (d, J = 2.9 Hz, 1H), 7.73 (d, J = 8.7 Hz, 1H), 7.88 (d, J = 0.95 Hz, 1H), 7.93 (d, J = 9.1 Hz, 2H), 8.11 (d, J = 6.6 Hz, 2H), 8.21 (d, J = 1.9 Hz, 1H), 10.84 (br s, 1H). MS-ESI$^+$ m/z 679 (M + 1). HPLC 98% pure at 220 nm.

7-Bromo-5-methylbenzo[1,2,4]triazin-3-ylamine 1-Oxide (22). A mixture of 4-bromo-2-methyl-6-nitroaniline (1 g, 4.33 mmol), cyanamide (0.5 g, 12 mmol), and pyridine hydrochloride (5 g, 43 mmol) was heated at 100 °C for 12 h. The reaction mixture was cooled, treated with 10% sodium hydroxide solution (4 mL, 10 mmol), and heated at 100 °C for 2 h. The reaction mixture was cooled to room temperature and filtered. The solid was washed with water (2 × 25 mL), acetone (2 × 5 mL), and diethyl ether (2 × 10 mL) to afford the title compound (0.4 g, 36%). ^{1} H NMR: δ 2.45 (s, 3 H), 7.49 (s, 2H), 7.81 (s, 1 H), 8.11 (d, J = 1.4 Hz, 1 H). MS-ESI$^+$ m/z 255 (M + 1).

7-Bromo-5-methyl-1,2,4-benzotriazin-3-amine (23). A solution of 7-bromo-5-methylbenzo[1,2,4]triazin-3-ylamine 1-oxide (**22**, 4.26 g, 16.7 mmol) and Raney nickel (10% by weight) in ethanol (160 mL) was stirred at room temperature under positive pressure of hydrogen for 10 h. The reaction mixture was filtered, concentrated, and purified using flash chromatography (SiO_2, 50% ethyl acetate in hexanes) to yield the title compound as a solid (3.9 g, 97%). ^{1}H NMR: δ 2.48 (s, 3H), 7.79 (br s, 3H), 8.25 (d, J = 1.8 Hz, 1H). MS-ESI$^+$ m/z 239 (M + 1).

7-(2-Chloro-5-methoxyphenyl)-5-methyl-1,2,4-benzotrizine-3-amine (24a). A solution of 7-bromo-5-methyl-1,2,4-benzotriazin-3-amine (**23**, 8 g, 33.5 mmol), 2-chloro-5-methoxyphenylboronic acid (9.3 g, 50.2 mmol), tetrakis(triphenylphosphine)palladium(0) (3.9 g, 3.3 mmol), and Na_2CO_3 (14.2 g, 134 mmol) in DME/EtOH/water (6:1:1, 335 mL) under argon was heated at 100 °C for 4 h. The reaction mixture was cooled to room temperature, diluted with dichloromethane (100 mL), filtered, and washed with water (3 × 100 mL) and ether (3 × 100 mL) to afford the title compound as a green solid (8.37 g, 84%). ^{1}H NMR: δ 2.54 (s, 3H), 3.82 (s, 3H), 7.03 (dd, J = 3.1, 8.8 Hz, 1H), 7.10 (d, J = 3.1 Hz, 1H), 7.50 (d, J = 8.8 Hz, 1H), 7.72 (br s, 2H), 7.74 (s, 1H), 8.07 (d, J = 1.8 Hz, 1H). MS-ESI$^+$ m/z 301 (M + 1).

7-Phenyl-5-methyl-1,2,4-benzotrizine-3-amine (24b). The title compound was obtained using the procedure described for **24a** in comparable yield. ^{1}H NMR: δ 2.57 (s, 3H), 7.30–7.50 (m, 3H), 7.66 (br s, 2H), 7.80−7.90 (m, 2H), 8.06 (dd, J = 1.1, 2.2 Hz, 1H), 8.29 (d, J = 1.8 Hz, 1H). MS-ESI$^+$ m/z 237 (M + 1).

7-(2-Chlorophenyl)-5-methyl-1,2,4-benzotrizine-3-amine (24c). A solution of 7-bromo-5-methyl-1,2,4-benzotriazin-3-amine (1 g, 4.18 mmol), 2-chlorophenylboronic acid (0.98 g, 6.28 mmol), tetrakis(triphenylphosphine)palladium(0) (0.483 g, 0.42 mmol), and sodium carbonate (1.77 g, 16.7 mmol) in dimethoxyethane/ethanol/water (6:1:1, 32 mL) was heated at reflux for 12 h. The reaction mixture was cooled, diluted with dichloromethane (30 mL), and filtered. The solid was washed with water (25 mL) and ether (25 mL) and dried to afford the title compound (0.32 g 28%). ^{1}H NMR: δ 2.54 (s, 3H), 7.40–7.50 (m, 2H), 7.56 (dd, J = 2.2, 7.1 Hz, 1H), 7.62 (dd, J = 2.2, 7.0 Hz, 1H), 7.72 (br s, 2H), 7.44 (s, 1H), 8.06 (d, J = 1.7 Hz, 1H). MS-ESI$^+$ m/z 271 (M + 1).

7-(2,6-Dimethylphenyl)-5-methyl-1,2,4-benzotrizine-3-amine (24d). The title compound was obtained using the procedure described for **24c** in comparable yield. ^{1}H NMR: δ 2.03 (s, 6H), 2.53 (s, 3H), 7.10−7.20 (m 3H), 7.46 (s, 1H), 7.61 (br s, 2H), 7.78 (d, J = 1.9 Hz, 1H). MS-ESI$^+$ m/z 265 (M + 1).

7-(2,6-Dichlorophenyl)-5-methyl-1,2,4-benzotrizine-3-amine (24e). The title compound was obtained using the procedure described for **24c** in comparable yield. ^{1}H NMR ($CDCl_3$): δ 2.53 (s, 3H), 7.49 (t, J = 7.8 Hz, 1H), 7.56 (t, J = 0.73 Hz, 1H), 7.63 (s, 1H), 7.65 (s, 1H), 7.77 (br s, 2H), 7.95 (d, J = 1.9 Hz, 1H). MS-ESI$^+$ m/z 305 (M + 1).

***tert*-Butyl 4-(4-Bromobenzoyl)piperazine-1-carboxylate (25c).** A solution of 4-bromobenzoyl chloride (1.0 g, 4.5 mmol), *tert*-butylpiperazine 1-carboxylate (1.1 g, 5.9 mmol), and triethylamine (1.5 mL, 11 mmol) in dichloromethane (15 mL) was stirred at room temperature for 15 h. The reaction mixture was diluted with ethyl acetate (100 mL), washed with saturated sodium bicarbonate solution (2 × 25 mL) and brine (2 × 25 mL), dried ($MgSO_4$), filtered, and concentrated under reduced pressure to give a tan solid. The solid was triturated in hexanes/diethyl ether (10:1 v/v) and washed with diethyl ether (25 mL) to afford the title compound as a white solid (1.6 g, 95%). ^{1} H NMR: δ 1.40 (s, 9H), 3.20–3.60 (m, 8H), 7.37 (d, J = 8.3 Hz, 2H), 7.65 (d, J = 8.4 Hz, 2H). MS-ESI$^+$ m/z 393 (M + Na).

1-[3-(4-Bromophenyl)propyl]pyrrolidine (25e). A solution of bromo-4-(3-bromopropyl)benzene (**27**, 3.5 g, 13 mmol), pyrrolidine (2.1 mL, 25 mmol), and cesium carbonate (8.2 g, 25 mmol) in dioxane (40 mL) was stirred at room temperature under argon for 15 h. The reaction mixture was poured onto water (200 mL) and extracted with ethyl acetate (3 × 100 mL). The organic layer was separated, washed with brine (2 × 50 mL), dried (Na_2SO_4), filtered, concentrated under reduced pressure, and purified by flash chromatography (SiO_2, 10−25% methanol in dichloromethane containing 2% triethylamine) to afford the title compound as a pale-orange oil (1.8 g, 53%). ^{1}H NMR: δ 1.60–1.65 (m, 6H), 2.35 (t, J = 7.3 Hz, 2H), 2.35–2.43 (m, 4H), 2.57 (t, J = 7.7 Hz, 2H), 7.16 (d, J = 8.3 Hz, 2H), 7.44 (d, J = 8.4 Hz, 2H). MS-ESI$^+$ m/z 268 (M + 1).

7-(2-Chloro-5-methoxyphenyl)-5-methyl-*N*-[4-(2-pyrrolidin-1-ylethoxy)phenyl]-1,2,4-benzotriazin-3-amine (26a). A solution of 7-(2-chloro-5-methoxyphenyl)-5-methyl-1,2,4-benzotrizine-3-amine (**24a**, 500 mg, 1.66 mmol), *N*-(2-chloroethyl)pyrrolidine (674 mg, 2.49 mmol), cesium carbonate (2.16 g, 6.65 mmol), tris(dibenzylideneacetone)dipalladium (152 mg, 0.17 mmol), and 4,5-bis(diphenylphosphino)-9,9-dimethyxanthene (xantphos, 287 mg, 0.50 mmol) in 1,4-dioxane (20 mL) was heated at reflux for 4 h under argon. The solid was filtered and washed with ethyl acetate (100 mL). The filtrate was washed with brine (1 × 100 mL). The organic solution was dried (Na_2SO_4), filtered, and concentrated under reduced pressure to 5 mL. Hexanes (50 mL) were added to the organic phase and the solid was filtered and purified by flash chromatography (SiO_2, using dichloromethane/methanol/28% aqueous ammonia, 100:10:2.5) to afford the title compound as a yellow solid (440 mg, 54%). ^{1}H NMR: δ 1.67–1.72 (m, 4H), 2.50–2.53 (m, 4H), 2.64 (s, 3H), 2.79 (t, J = 11.8 Hz, 2H), 3.83 (s, 3H), 4.07 (t, J = 5.9 Hz, 2H), 7.00 (d, J = 9.1 Hz, 2H), 7.04 (dd, J = 3.0, 4.4 Hz, 1H), 7.13 (d, J = 3.0 Hz, 1H), 7.52 (d, J = 8.9 Hz, 1H), 7.85 (d, J = 0.7 Hz, 1H), 7.92 (d, J = 9.0 Hz, 1H), 8.17 (d, J = 1.5 Hz, 1H), 10.81 (br s, 1H). MS-ESI$^+$ m/z 490 (M + 1).

4-{[7-(2-Chloro-5-methoxyphenyl)-5-methyl-1,2,4-benzotriazin-3-yl]amino}-*N*-(2-pyrrolidin-1-ylethyl)benzenesulfonamide (26b). A solution of 7-(2-chloro-5-methoxyphenyl)-5-methyl-1,2,4-benzotrizine-3-amine (**24a**, 0.157 g, 0.523 mmol), 4-bromo-*N*-(2-pyrrolidin-1-ylethyl)benzenesulfonamide (0.261 g, 0.785 mmol), cesium carbonate (0.512 g, 1.57 mmol), 4,5-bis(diphenylphosphino)-9,9-dimethylxanthene (0.061 g, 0.10 mmol), and tris(dibenzylideneacetone)dipalladium (0.048 g, 0.052mmol) in dioxane (5 mL) was flushed with argon and heated at reflux for 18 h. The hot reaction mixture was filtered, diluted with ethyl acetate, and washed with brine. The organic layer was dried (Na_2SO_4), filtered, and evaporated to provide a solid. The solid was dissolved in dichloromethane and precipitated with hexanes to afford a yellow powder (0.276 g, 95% yield). ^{1}H NMR: δ 1.63–1.67 (m, 4H), 2.35–2.42 (br s, 4H), 2.47 (br s, 2H), 2.71 (s, 3H), 2.87 (t, J = 6.9 Hz, 2H), 3.83 (s, 3H), 7.06 (dd, J = 3.1, 8.9 Hz, 1H), 7.14 (d, J = 3.1 Hz, 1H), 7.53 (d, J = 8.9 Hz, 1H), 7.84 (d, J = 5.1 Hz, 2H), 7.95 (d, J = 0.9 Hz, 1H), 8.21 (d, J = 5.2 Hz, 2H), 8.27 (d, J = 1.8 Hz, 1H), 11.39 (s, 1H). MS-ESI$^+$ m/z 553.3 (M + 1).

***tert*-Butyl 4-(4-{[7-(2-Chloro-5-methoxyphenyl)-5-methyl-1,2,4-benzotriazin-3-yl]amino}benzoyl)piperazine-1-carboxylate (26c).** A suspension of 7-(2-chloro-5-methoxyphenyl)-5-methylbenzo[1,2,4]triazin-3-ylamine (0.10 g, 0.33 mmol), *tert*-butyl 4-(4-bromobenzoyl)-piperazine-1-carboxylate (0.16 g, 0.44 mmol), palladium acetate

(4 mg, 0.018 mmol), xantphos (20 mg, 0.035 mmol), and potassium *tert*-butoxide (0.10 g, 0.89 mmol) in xylene (3 mL) was heated in a microwave reactor at 160 °C for 15 min. After cooling to room temperature, the mixture was filtered and the solids were washed with dichloromethane. The filtrate was concentrated and purified using flash chromatography (SiO_2, 40% ethyl acetate in hexanes) to afford the title compound as an orange solid (45 mg, 23%). ^{1}H NMR: δ 1.42 (s, 9H), 2.70 (s, 3H), 3.35–3.45 (m, 4H), 3.45–3.55 (m, 4H), 3.84 (s, 3H), 7.06 (dd, $J = 2.9$, 8.7 Hz, 1H), 7.15 (d, $J = 2.9$ Hz, 1H), 7.49 (d, $J = 8.7$ Hz, 1H), 7.53 (d, $J = 8.7$ Hz, 2H), 7.93 (t, $J = 1.0$ Hz, 1H), 8.11 (d, $J = 8.6$ Hz, 2H), 8.25 (d, $J = 1.7$ Hz, 1H), 11.21 (s, 1H). MS-ESI$^+$ *m/z* 589 (M + 1).

Benzyl 4-[(4-{[7-(2-Chloro-5-methoxyphenyl)-5-methyl-1,2-4-benzotriazin-3-yl]amino}phenyl)sulfonyl]piperdine-1-carboxylate (26d). A solution of 7-(2-chloro-5-methoxyphenyl)-5-methylbenzo[1,2,4]triazin-3-ylamine (0.13 g, 0.44 mmol), benzyl 4-(4-bromobenzenesulfonyl)piperdine-1-carboxylate (0.232 g, 0.53 mmol), cesium carbonate (0.432 g, 1.33 mmol), 4,5-bis(diphenylphosphino)-9,9-dimethylxanthane (0.051 g, 0.088 mmol), and tris(dibenzylideneacetone)dipalladium (0.04 g, 0.044 mmol) in dioxane (12 mL) was heated at reflux under argon for 18 h. The reaction mixture was cooled and diluted with water (12 mL). The solid was filtered and washed with water (20 mL) and ether (20 mL) to afford the title compound as a yellow solid (0.27 g, 93% yield). MS-ESI$^+$ *m/z* 658 (M + 1).

Bromo-4-(3-bromopropyl)benzene (27). Triphenylphosphine (6.3 g, 24 mmol) and then carbon tetrabromide (8.0 g, 24 mmol) were added to a solution of bromo-4-(3-hydroxypropyl)benzene (4.0 g, 19 mmol) in tetrahydrofuran (30 mL) at 0 °C under an argon atmosphere. The mixture was stirred at 0 °C for 15 min and then at room temperature for an additional 15 h. The solvent was removed under reduced pressure and purified by flash chromatography (SiO_2, hexanes) to afford the title compound as a colorless oil (3.5 g, 66%). ^{1} H NMR: δ 2.03–2.12 (m, 2H), 2.68 (t, $J = 7.5$ Hz, 2H), 3.49 (t, $J = 6.5$ Hz, 2H), 7.19 (d, $J = 8.3$ Hz, 2H), 7.47 (d, $J = 8.3$ Hz, 2H). MS-ESI$^+$ *m/z* 279 (M + 1).

4-Chloro-3-(5-methyl-3-{[4-(2-pyrrolidin-1-ylethoxy)phenyl]amino}-1,2,4-benzotriazin-7-yl)phenyl-*N*-butyloxycarbonyl Glycinate (28). A solution of 4-chloro-3-(5-methyl-3-{[4-(2-pyrrolidin-1-ylethoxy)phenyl]amino}-1,2,4-benzotriazin-7-yl)phenol (**5**, 0.25 g, 0.526 mmol), *N*-*tert*-butyloxycarbonylglycine (0.37 g, 2.11 mmol), *N*-(3-dimethylaminopropyl)-*N*′-ethylcarbodiimide hydrochloride (1 g, 5.26 mmol), and 4-dimethylaminopyridine (65 mg, 0.526 mmol) in dimethylformamide (25 mL) was stirred at room temperature for 18 h. The reaction mixture was concentrated and purified by flash chromatography (SiO_2, 10% methanol in dichloromethane) to afford the title compound (0.085 g, 26%). ^{1}H NMR: δ 1.39 (s, 9H), 1.87–1.88 (m, 4H), 2.64 (s, 3H), 3.10–3.14 (m, 4H), 4.00 (d, $J = 5.9$ Hz, 2H), 4.29 (t, $J = 4.7$ Hz, 2H), 7.06 (d, $J = 8.9$ Hz, 2H), 7.26 (dd, $J = 2.8$, 8.7 Hz, 1H), 7.39 (d, $J = 2.7$ Hz, 1H), 7.46 (t, $J = 6.0$ Hz, 1H), 7.70 (d, $J = 8.7$ Hz, 1H), 7.85 (t, $J = 0.9$ Hz, 1H), 7.96 (d, $J = 9.0$ Hz, 2H), 8.18 (s, 1H), 10.89 (s, 1H). MS-ESI$^+$ *m/z* 633 (M + 1).

Chemical Stability Studies of Prodrugs 10–20. Chemical stability of various prodrugs (**10**−**20**) was measured in a formulation solution containing 0.5% of compounds and 0.5% HPMC/5% dextrose at pH 6.7. The vials were closed and heated in an autoclave at 120 °C for 1 h. The solutions were cooled to room temperature and analyzed on Shimadzu HPLC systems equipped with LC-10ATvp pumps, SIL-10ADvp autoinjector, SPD-M10Avp diode array, an ELSD-LT detectors, and Agilent C-18 Zorbax 250 mm × 4.6 mm column with 5 μm particle size. The analytical gradient consisted of 15% acetonitrile in water ramping up to 90% acetonitrile, both containing 0.05% trifluoroacetic acid.

Hydrolysis of Prodrugs in Rabbit Eye Homogenates. Two eyeballs (6.37 g) from a Dutch-Belted rabbit were collected and homogenized in 20 mL of 1× radioimmunoprecipitation (RIPA) buffer (diluted from 10× RIPA buffer, Upstate Biotechnology, Inc. Charlottesville, VA). Prodrugs **12**, **14**, **18**, and **19** were dissolved in dimethyl sulfoxide (1 mg/mL) and added to 3 mL of the homogenate solution with a final concentration of 5 μg/mL. The solutions were kept at 37 °C. The homogenates were sampled at 0, 0.25, 1, 2, and 6 h. The reaction of one aliquot of the mixtures was terminated at the above time points by addition of an equal volume of cold acetonitrile (with 1 μM of the internal standard) and centrifugation. The acetonitrile was collected and analyzed immediately. Rate of hydrolysis of prodrugs was conducted by measuring the conversion of prodrugs to **5** in extracts of ocular tissues. Compounds **12**, **14**, **18**, and **19** incubated in RIPA buffer at 37 °C for 120 min were used as controls. The supernatants of reaction mixtures were analyzed for prodrugs (**12**, **14**, **18**, and **19**) and **5**. The samples were analyzed using API3000 liquid chromatography equipped with an MS/MS (triple quadrupole) spectrometer, Zorbax SB 75 mm × 2.1 mm, 3.5 μm column at 40 °C, using water and acetonitrile as mobile phase, both containing 0.05% trifluoroacetic acid. Hydrolysis rates were calculated using first-order kinetics.

Structure Based Modeling Studies. While several crystal structures of the unphosphorylated form of Src are available (PDB codes 2src, 1fmk, 1y57, 2ptk), it is known that kinases in the Src family undergo conformational change upon phosphorylation, casting doubt on the relevance of these crystal forms to drug discovery. We felt that the crystal structure of the inactive form of Src is not useful for modeling studies. The fully activated catalytic domain of human Src kinase was built on the basis of available crystal structures of activated Lck. The catalytic domains of Src and Lck exhibit 67% sequence identity over 273 residues without gaps in the alignment with significantly higher homology exhibited in the ATP binding site. The model was built using the interactive programs InsightII and Homology from Accelrys. Compound **5** was docked initially into the active site using an automated modeling program BioDock (NIH SBIR Grant 1R43GM071055) and subsequently using interactive modeling in InsightII. Models with and without ligands were subjected to energetic refinement including solvent using the Accelerys program Discover. Visualization was generated using the program BioInterpreter (NIH SBIR Grant 5R44GM061465). After comparison of available crystal structures for VEGFr2 (1ywn, 1vr2, 1y6a, and 1y6b), the 1ywn crystal structure was selected for modeling because of its closest resemblance to protein used in enzymatic assay. When **5** was docked into the pocket, it exhibited a critical hydrogen bond from the hydroxyphenyl of **5** to Glu885 on the αC-helix residue on the protein.

In Vitro Src Kinase Inhibition Assay. The IC_{50} values for compounds were determined using a luminescence-based kinase assay with recombinant Src obtained from Invitrogen. In white, flat-bottomed 96-well plates (Nunc) parallel assays were run at room temperature at a final volume of 50 μL. Each well contained 40 μL of buffer consisting of 40 mM Tris buffer, pH 7.4, containing 50 mM $MgCl_2$, 800 μM EDTA, 350 μM Triton X-100, 2 mM β-mercaptoethanol, 250 μM peptide substrate (PTK2, Promega), and an appropriate amount of Src (75–25 ng/well) such that the assay was linear over 60 min. The final concentrations of compounds for IC_{50} value determinations ranged from 1000 to 0.01 μM by adding the appropriate amount of compound in 2.5 μL of DMSO; the DMSO present in each assay was constant at 5%. The reaction was initiated by the addition of 10 μL of ATP to a final assay concentration of 3 μM. After the reaction had proceeded for 60 min, 50 μL of Kinase-Glo reagent (Promega) was added to terminate the reaction. This solution was then allowed to proceed for an additional 10 min to maximize the luminescence reaction. Values were then measured using an Ultra 384 instrument (Tecan) set for luminosity measurements. Two control reactions were also run: one reaction containing no compound and the second containing neither inhibitor nor peptide substrate. IC_{50} values were derived from experimental data using the nonlinear curve fitting capabilities of Prism (version 4, GraphPad Software).

In Vitro VEGFr2 Kinase Inhibition Assay. The IC_{50} values for compounds were determined using a luminescence-based kinase assay with recombinant VEGFr2 obtained from Invitrogen. In white, flat-bottomed 96-well plates (Nunc) parallel assays were run at room temperature at a final volume of 50 μL. Each well contained 40

μL of buffer consisting of 40 mM Tris buffer, pH 7.4, containing 50 mM $MgCl_2$, 800 μM EDTA, 350 μM Triton X-100, 2 mM β-mercaptoethanol, 500 μg/mL poly-E4Y (Sigma) for VEGFr2 and an appropriate amount of VEGFr2 such that the assay was linear over 60 min. The final concentrations of compounds for IC_{50} value determinations ranged from 10 to 0.001 μM by adding the appropriate amount of compound in 2.5 μL of DMSO; the DMSO present in each assay was constant at 5%. The reaction was initiated by the addition of 10 μL of ATP to a final assay concentration of 3 μM. After the reaction had proceeded for 60 min, 50 μL of Kinase-Glo reagent (Promega) was added to terminate the reaction. This solution was then allowed to proceed for an additional 10 min to maximize the luminescence reaction. Values were then measured using an Ultra 384 instrument (Tecan) set for luminosity measurements. Two control reactions were also run: one reaction containing no compound and the second containing neither inhibitor nor peptide substrate. IC_{50} values were derived from experimental data using the nonlinear curve fitting capabilities of Prism (version 4, GraphPad Software).

In Vitro YES Kinase Inhibition Assay. The IC_{50} values for compounds were determined using a luminescence-based kinase assay with recombinant YES obtained from Invitrogen. In white, flat-bottomed 96-well plates (Nunc) parallel assays were run at room temperature at a final volume of 50 μL. Each well contained 40 μL of buffer consisting of 40 mM Tris buffer, pH 7.4, containing 50 mM $MgCl_2$, 800 μM EDTA, 350 μM Triton X-100, 2 mM β-mercaptoethanol, 250 μM peptide substrate (PTK2, Promega), and an appropriate amount of YES (75–25 ng/well) such that the assay was linear over 60 min. The final concentrations of compounds for IC_{50} value determinations ranged from 1000 to 0.01 μM by adding the appropriate amount of compound in 2.5 μL of DMSO; the DMSO present in each assay was constant at 5%. The reaction was initiated by the addition of 10 μL of ATP to a final assay concentration of 3 μM. After the reaction had proceeded for 60 min, 50 μL of Kinase-Glo reagent (Promega) was added to terminate the reaction. This solution was then allowed to proceed for an additional 10 min to maximize the luminescence reaction. Values were then measured using an Ultra 384 instrument (Tecan) set for luminosity measurements. Two control reactions were also ran: one reaction containing no compound and the second containing neither inhibitor nor peptide substrate. IC_{50} values were derived from experimental data using the nonlinear curve fitting capabilities of Prism (version 4, GraphPad Software).

In Vitro VEGF-Mediated Proliferation in Human Retinal Microvascular Endothelial Cell Assay. For the cellular proliferation assays, human retinal microvascular endothelial cells (Cell Systems; Kirkland, WA) were plated at a density of $\sim 1.5 \times 10^3$ cells/well in a 96-well plate (Corning; Corning, NY) and allowed to adhere for approximately 5–6 h. Medium was then changed into CSC-Maintenance Medium (Cell Systems; Kirkland, WA) and incubated for approximately 48 h at 37 °C/5% CO_2. As indicated by the manufacturer, this specialized medium contains 10% FBS but no growth factor and renders proliferating cells into a quiescent state. The cells were then pretreated with varying concentrations of **5** (5−0.00229 or 2−0.00195 μM) or DMSO (as a vehicle control) prepared in basal CSC medium containing 10% FBS and 50 μg/mL heparin for approximately 60 min at 37 °C/5% CO_2. Human recombinant VEGF (Peprotech; Rocky Hill, NJ) was then added to a final concentration of 50 ng/mL, and cells were incubated for 48 h, at which time cell proliferation was quantified using the Cell Proliferation Kit (Roche; Alameda, CA) as described by the manufacturer. Briefly, for one 96-well plate, 100 μL of electron-coupling reagent was added to 5 mL of XTT labeling solution. A 50 μL sample of this solution was then added to each well, and the reaction was allowed to develop at 37 °C/5% CO_2. The colored formazan product that is generated by metabolically active cells was measured spectrophotometrically using the SpectraMax spectrophotometer (Molecular Devices; Sunnyvale, CA) at 492 nm with correction at 690 nm. IC_{50} values were determined using the GraphPad Prism 4.0 software (San Diego, CA), with the corrected absorbance values plotted on *y*-axis (linear scale) and logarithmic values of concentration (μM) on the *x*-axis. Data were subjected to a nonlinear regression fit analysis and the concentrations at which endothelial cell proliferation was inhibited by 50% determined.

Pharmacokinetic Studies of 12 in Mouse Ocular Tissue after a Single Topical Instillation. The 0.7% w/v formulation of **5** was prepared as follows. The hydrochloride salt of **5** (31.16 mg) was mixed with PL90G liposome (970 mg) and dissolved in ethanol (2 mL). The solution was evaporated to dryness under reduced pressure and resuspended in water (2.7 g) containing 3% (w/v) propylene glycol. The solution pH was adjusted to 6.1 with 1 N NaOH, the mixture was homogenized using a sonicator probe (model GE-130), the osmolality of the solution was adjusted to 355 mOsm, and the mixture was filtered through a 0.22 μm PVDF syringe filter (Millipore). The 1.8% w/v formulations of **12** was prepared as follows. Compound **12** (26.44) was mixed with PL90G liposome (386.97 mg) and dissolved in 2 mL of ethanol. The solution was evaporated to dryness under reduced pressure and resuspended in water (923.55 mg) containing 3% (w/v) propylene glycol. The pH was adjusted to 6.2 with 1 N HCl. The mixture was homogenized using a sonicator probe (model GE-130), and osmolality was adjusted to 327 mOsm and filtered through a 0.45 μm PVDF syringe filter (Millipore). Twenty male mice (C57BL/6) were given one 10 μL drop of 0.7% of **5**. Composite sampling was employed to generate tissue concentration−time profiles for **5** over the following time course (N = 4/time point): 0.5, 1, 3, 7, and 24 h postinstillation. Both eyes were removed from each mouse and dissected to obtain the cornea, retina, and eye cup (sclera and choroid). Plasma samples were also obtained from each mouse at the time of euthanasia. Ten male mice were given one 10 μL drop of the solution of **12**. Composite sampling was employed to generate tissue concentration−time profiles for **12** and **5** over the following time course (N = 2/time point): 0.5, 1, 3, 7, and 24 h postinstillation. Both eyes were removed from each mouse and dissected to obtain the cornea, retina, and eye cup. Plasma samples were also obtained from each mouse at the time of euthanasia. Individual eye tissue samples were combined and weighed. The weighed tissues were homogenized in 0.5 mL of RIPA buffer using FP120 FastPrep (ThermoSavant) and extracted with 0.5 mL of acetonitrile (containing internal standard). The supernatants (800 μL) were dried and reconstituted into 400 μL of 8:2 dimethyl sulfoxide (DMSO)/water for analysis. Plasma samples were extracted by addition of a 2-fold excess of acetonitrile containing internal standard followed by centrifugation. The supernatants were isolated for analysis. Processed plasma and ocular tissue samples were quantitated by LC/MS/MS against externals calibration standards prepared in naive mouse tissues. Matrix calibration standards and quality control (QC) samples were prepared by adding stock solutions of **5** or **12** into a series of aliquots of blank mouse plasma (for plasma analysis) or blank mouse ocular tissue (for ocular tissue analysis). The final concentrations ranged from 0.5 to100 ng/mL for plasma analyses and from 0.125 to 500 ng/mL for ocular tissue analyses.

The LC/MS/MS system consisted of an Sciex API3000 triple quadrupolar mass spectrometer (MDS Sciex), an Agilent 1100 HPLC system (Agilent Technologies, Inc.), and a CTC autosampler (Leap Technologies). The LC separations were performed on a Zorbax SB 75 mm × 2.1 mm, 3.5 μm reverse phase HPLC column (Agilent Technologies, Inc.). The column temperature was kept at 40 °C. Mobile phase A consisted of 0.05% trifluoroacetic acid (TFA) in water, and mobile phase B consisted of 0.05% TFA in acetonitrile. The flow rate was kept constant at 0.25 mL/min. Following a 30 μL sample injection, mobile B was held at 5% for 3 min followed by a linear increase to 70% mobile phase B over 5 min. The mass spectrometric detection of **12** and **5** was achieved using electrospray ionization operating in positive ionization mode. The molecular ion transitions of *m/z*: 476.18 → 98.2 and *m/z*: 580.17 → 98.2 were monitored in MRM mode for **5** and **12**, respectively. Pharmacokinetic parameters were estimated using WinNonlin (version 4.1) based on mean concentrations for each time point and individual tissue. The time to maximum concentration (T_{max}) and the maximum concentration (C_{max}) were determined on the basis of measured concentrations. The area under the curve, AUC_{last}, was

calculated from mean concentration data using the linear trapezoidal rule. No standard deviations are given, since the data represent the combined exposure from only two to four eyes.

Laser-Induced Choroidal Neovascularization in Mice. Compound **12** was prepared as a solution as described above. Laser-photocoagulation-induced rupture of Bruch's membrane was used to generate CNV as previously described.[43] Briefly, 4- to 5-week-old female C57BL/6J mice were anesthetized with ketamine hydrochloride (100 mg/kg body weight), and the pupils were dilated with 1% tropicamide (Alcon Laboratories, Inc.; Forth Worth, TX). Three burns of 532 nm diode laser photocoagulation (75 μm spot size, 0.1 s duration, 120 mW) were delivered to each retina by using the slit lamp delivery system of a photocoagulator (OcuLight, Iridex; Mountain View, CA) and a hand-held coverslip as a contact lens. Burns were performed in the 9, 12, and 3 o'clock positions of the posterior pole of the retina. Production of a bubble at the time of laser treatment, which indicates rupture of Bruch's membrane, is an important factor in obtaining CNV.[43] Only burns in which a bubble was produced were included in the study. Body weights were monitored throughout the experiment, and the CNV area was measured on day 14 as described below. For topical administration, eight mice/group were given one 10 μLdrop of the formulation vehicle, 0.61% w/v **12**, or 1.83% w/v **12** three times a day (t.i.d.), with each dose separated by 4 h and no treatment in the fellow eye. One group of mice had a rupture to Bruch's membrane and no treatment to either eye. Two weeks after the rupture of Bruch's membrane, mice were anesthetized and perfused with fluorescein-labeled dextran (2×10^6 average molecular weight, Sigma-Aldrich; St. Louis, MO) and choroidal flatmounts were prepared as previously described.[43] Briefly, the eyes were removed and fixed for 1 h in 10% phosphate-buffered formalin and the cornea and lens were removed. The entire retina was carefully dissected from the eye cup. Radial cuts were made from the edge of the eye cup to the equator in all four quadrants and flat-mounted in aqueous mounting medium (Aquamount, BDH; Poole, U.K.). Flat-mounts were examined by fluorescence microscopy (Axioskop, Carl Zeiss Meditec; Thornwood, NY), and images were digitized with a three charge coupled device (CCD) color video camera (IK-TU40A, Toshiba; Tokyo, Japan) and a frame grabber. Image-analysis software (Image-Pro Plus, Media Cybernetics; Silver Spring, MD) was used to measure the area of each CNV lesion. Statistical comparisons were made using a linear mixed model.[59] Probabilities for comparison of treatments were adjusted for multiple comparisons by the Dunnett method.[47]

Acknowledgment. The authors thank Barbara Robinson and Linda Hwang for valuable discussions and technical assistance.

Supporting Information Available: Elemental analysis results and details of the effects of **5** on target kinases and topically applied **5** and **12**. This material is available free of charge via the Internet at http://pubs.acs.org.

References

(1) De Jong, P. T. Age-related macular degeneration. *N. Engl. J. Med.* **2006**, *355*, 1474–1485.

(2) Rattner, A.; Nathans, J. Macular degeneration: recent advances and therapeutic opportunities. *Nat. Rev. Neurosci.* **2006**, *7*, 860–872.

(3) Shweiki, D.; Itin, A.; Soffer, D.; Keshet, E. Vascular endothelial growth factor induced by hypoxia may mediate hypoxia-initiated angiogenesis. *Nature* **1992**, *359*, 843–845.

(4) Forsythe, J. A.; Jiang, B. H.; Iyer, N. V.; Faton, A.; Leung, S. W.; Koos, R. D.; Semenza, G. L. **Activation of vascular endothelial growth factor gene transcription by hypoxia-inducible factor 1. *Mol. Cell. Biol.* **1996**, *16*, 4604–4613.

(5) Aiello, L. P.; Avery, R. L.; Arrigg, P. G.; Keyt, B. A.; Jampel, H. D.; Shah, S. T.; Pasquale, L. R.; Thieme, H.; Iwamoto, M. A.; Park, J. E.; Nguyen, H. V.; Aiello, L. M.; Ferrara, N.; King, G. L. Vascular endothelial growth factor in ocular fluid of patients with diabetic retinopathy and other retinal disorders. *N. Engl. J. Med.* **1994**, *331*, 1480–1487.

(6) Pe'er, J.; Shweiki, D.; Itin, A.; Hemo, I.; Gnessin, H.; Keshet, E. Hypoxia-induced expression of vascular endothelial growth factor by retinal cells is a common factor in neovascularizing ocular diseases. *Lab. Invest.* **1995**, *72*, 638–645.

(7) Wand, F.; Rendahl, K. G.; Manning, W. C.; Quiroz, D.; Coyne, M.; Miller, S. S. AAV-mediated expression of vascular endothelial growth factor induces choroidal neovascularlaztion in rat. *Invest. Ophthalmol. Visual Sci.* **2003**, *44*, 781–790.

(8) Reich, S. J.; Fosnot, J.; Kuroki, A.; Tang, W.; Yang, X.; Maguire, A. M.; Bennett, J.; Tolentino, M. J. Small interfering RNA (siRNA) targeting VEGF effectively inhibits ocular neovascularization in a mouse model. *Mol. Vision* **2003**, *9*, 210–216.

(9) Bainbridge, J. W.; Jia, H.; Bagherzadeh, A.; Selwood, D.; Ali, R. R.; Zachary, I. A peptide encoded by exon 6 of VEGF (EG3306) inhibits VEGF-induced angiogenesis in vitro and ischaemic retinal neovascularisation *in vivo*. *Biochem. Biophys. Res. Commun.* **2003**, *302*, 793–799.

(10) Aiello, L. P.; Pierce, E. A.; Foley, E. D.; Takagi, H.; Chen, H.; Riddle, L.; Ferrara, N.; King, G. L.; Smith, L. E. Suppression of retinal neovascularization in vivo by inhibition of vascular endothelial growth factor (VEGF) using soluble VEGF-receptor chimeric proteins. *Proc. Natl. Acad. Sci. U.S.A.* **1995**, *92*, 10457–10461.

(11) Ferrara, N.; Damico, L.; Shams, N.; Lowman, H.; Kim, R. Development of ranibizumab, an anti-vascular endothelial growth factor antigen binding fragment, as therapy for neovascular age-related macular degeneration. *Retina* **2006**, *26*, 859–870.

(12) Rosenfeld, P. J.; Brown, D. M.; Heier, J. S.; Boyer, D. S.; Kaiser, P. K.; Chung, C. Y.; Kim, R. Y. Ranibizumab for neovascular age-related macular degeneration. *N. Engl. J. Med.* **2006**, *355*, 1419–1431.

(13) Brown, D. M.; Kaiser, P. K.; Michels, M.; Soubrane, G.; Heier, E. S.; Kim, R. Y.; Sy, J. P.; Schneider, S. Ranibizumab versus verteporfin for neovascular age-related macular degeneration. *N. Engl. J. Med.* **2006**, *355*, 1432–1444.

(14) Nguyen, Q. D.; Tatlipinar, S.; Shah, S. M.; Haller, J. A.; Quinlan, E.; Sung, J.; Zimmer-Galler, I.; Do, D. V.; Campochiaro, P. A. Vascular endothelial growth factor is a critical stimulus for diabetic macular edema. *Am. J. Ophthalmol.* **2006**, *142*, 961–969.

(15) Fernando, N. H.; Hurwitz, H. I. Targeted therapy of colorectal cancer: clinical experience with bevacizumab. *Oncologist* **2004**, *1*, 1–18.

(16) Saishin, Y.; Saishin, Y.; Takahashi, K.; Silva, R. L.;E.; Hylton, D.; Rudge, J. S.; Wiegand, S. J.; Campochiaro, P. A. VEGF-TRAPR1R2 suppresses choroidal neovascularization and VEGF-induced breakdown of the blood−retinal barrier. *J. Cell. Physiol.* **2003**, *195*, 241–248.

(17) Sirna Therapeutics is currently developing an injectable form of SiRNA (Sirna-027) targeting VEGFr. Shen, J.; Samul, R.; Silva, R. L.; Akiyama, H.; Liu, H.; Saishin, Y.; Hackett, S. F.; Zinnen, S.; Kossen, K.; Fosnaugh, K.; Vargeese, C.; Gomez, A.; Bouhana, K.; Aitchison, R.; Pavco, P.; Campochiaro, P. A. Suppression of ocular neovascularization with siRNA targeting VEGF receptor 1. *Gene Ther.* **2005**, *13*, 225–234.

(18) Small molecules targeting VEGFr pathway for the treatment of AMD are under development at Pfizer. Beals, C. R.; Day, W. W.; Khalil, D. A.; Klamerus, K. J.; Raber, S. R.; Scassellati-Sorzolini, B.; Zwillich, S. H. Compositions Comprising Indazole Compound for Sub-Tenon Delivery. WO 2006117666, April 2006.

(19) Orally delivered vatalanib is being evaluated in a phase II clinical trial along with verteporfin in patients with subfoveal choroidal neovascularization (CNV) secondary to age-related macular degeneration. http://www.clinicaltrials.gov/ct/gui/show/NCT00138632.

(20) Several devices are in development to deliver drugs to the back of the eye. Sultana, Y; Jain, R.; Aqil, M.; Ali, A. *Curr. Drug Delivery* **2006**, *3*, 207–217.

(21) Antismoking compound mecamylamine targeting endothelial nicotinic acetylcholine receptor and pazopanib from GlaxoSmithKline targeting VEGFr are in phase I. http://clinicaltrials.gov/ct/show/NCT00463320?order=19.

(22) A VEGF trap agent from Regeneron Pharmaceuticals, Inc. and Bayer Health Care AG is in Phase II. Saishin, Y.; Saishin, Y.; Takahashi, K.; Silva, R. L.; Hylton, D.; Rudge, J. S.; Wiegand, S. J.; Campochiaro, P. A. VEGF-TRAPR1R2 suppresses choroidal neovascularization and VEGF-induced breakdown of the blood−retinal barrier. *J. Cell. Physiol.* **2003**, *195*, 241–248.

(23) Othera Pharmaceuticals, Inc. is developing OT-551 targeting NF-κB mediated transcriptional activation for the treatment of AM. Tanito, M.; Li, F.; Elliott, M. H; Dittmar, M.; Anderson, R. E. Protective effect of TEMPOL derivatives against light-induced retinal damage in rats. *Invest. Ophthalmol. Visual Sci.* **2007**, *48*, 1900–1905.

(24) Weis, S.; Cui, J.; Barnes, L.; Cheresh, D. Endothelial barrier disruption by VEGF-mediated Src activity potentiates tumor cell extravasation and metastasis. *J. Cell Biol.* **2004**, *167*, 223–229.

(25) Eliceiri, B. P.; Puente, X. S.; Hood, J. D.; Stupack, D. G.; Schlaepfer, D. D.; Huang, X. Z.; Sheppard, D.; Cheresh, D. A. Src-mediated coupling of focal adhesion kinase to integrin $\alpha v\beta 5$ in vascular endothelial growth factor signaling. *J. Cell Biol.* **2002**, *157*, 149–159.
(26) Personal communication Martin Friedlander, Department of Cell Biology, Scripps Clinic Torry Pines 10666 North Torrey Pines Road, MS214, The Scripps Research Institute, La Jolla, CA 92037.
(27) Thomas, S. M.; Brugge, J. S. Cellular functions regulated by Src family kinases. *Annu. Rev. Cell Dev. Biol.* **1997**, *13*, 513–609.
(28) Eliceiri, B. P.; Paul, R.; Schwartzberg, P. L.; Hood, J. D.; Leng, J.; Cheresh, D. A. Selective requirement for Src kinases during VEGF-induced angiogenesis and vascular permeability. *Mol. Cell* **1999**, *4*, 915–924.
(29) Noronha, G.; Barrett, K.; Cao, J.; Dneprovskaia, E.; Fine, R.; Gong, X.; Gritzen, C.; Hood, J.; Kang, X.; Klebansky, B.; Lohse, D.; Mak, C. C.; McPherson, A.; Palanki, M. S. S.; Pathak, V. P.; Renick, J.; Soll, R.; Splittgerber, U.; Wrasidlo, W.; Zeng, B.; Zhao, N. Discovery and preliminary structure activity relationship studies of novel benzotriazine based compounds as Src inhibitors. *Bioorg. Med. Chem. Lett.* **2006**, *16*, 5546–5550.
(30) Noronha, G.; Barrett, K.; Boccia, A.; Brodhag, T.; Cao, J.; Chow, C. P.; Dneprovskaia, E.; Doukas, J.; Fine, R.; Gong, X.; Gritzen, C.; Gu, H.; Hanna, E.; Hood, J. D.; Hu, S.; Kang, X.; Key, J.; Klebansky, B.; Kousba, A.; Li, G.; Lohse, D.; Mak, C.; McPherson, A.; Palanki, M. S. P.; Pathak, V. P.; Renick, J.; Shi, F.; Soll, R.; Splittgerber, U.; Stoughton, S; Tang, S.; Yee, S.; Zeng, B.; Zhao, N.; Zhu., H. Discovery of [7-(2,6-dichlorophenyl)-5-methylbenzo[1,2,4]triazin-3-yl]-[4-(2-pyrrolidin-1-ylethoxy)phenyl]amine, a potent, orally active Src kinase inhibitor with anti-tumor activity in preclinical assays. *Bioorg. Med. Chem. Lett.* **2007**, *17*, 602–608.
(31) Wolf, F. J.; Pfister, K., III; Wilson, R. M., Jr.; Robinson, C. A.; Benzotriazines, I. A new series of compounds having antimalarial activity. *J. Am. Chem. Soc.* **1954**, *76*, 3551–3553.
(32) Mason, J. C.; Tennant, G. *J. Chem. Soc. B* **1970**, 911–916.
(33) Kudo, N.; Perseghini, M.; Fu, G. C. *Angew. Chem., Int. Ed.* **2006**, *45*, 1282–1284.
(34) Tundel, R. E.; Anderson, K. W.; Buchwald, S. L. *J. Org. Chem.* **2006**, *71*, 430–433.
(35) Zhu, X.; Kim, J. L.; Newcomb, J. R.; Rose, P. E.; Stover, D. R.; Toledo, L. M.; Zhao, H.; Morgenstern, K. A. Structural analysis of the lymphocyte-specific kinase Lck in complex with non-selective and Src family selective kinase inhibitors. *Structure* **1999**, *7*, 651–66. PDB entry 1qpe.
(36) Breitenlechner, C. B.; Kairies, N. A.; Honold, K.; Scheiblich, S.; Koll, H.; Greiter, E.; Koch, S.; Schafer, W.; Huber, R.; Engh, R. A. Crystal structures of active SRC kinase domain complexes. *J. Mol. Biol.* **2005**, *353*, 222–231 (PDB entries 1yom, 1yol, 1yoj).
(37) After we had completed our work in the benzotriazines targeting Src, Abl, and Abl-T315I, a paper from Ariad targeting Src by utilizing the Glu310 in the back of the hydrophobic pocket by making a donor interaction was published: Dalgarno, D.; Stehle, T.; Narula, S.; Schelling, P.; Schravendijk, M. R. V.; Adams, S.; Andrade, L.; Keats, J.; Ram, M.; Jin, L.; Grossman, T.; MacNeil, I.; Metcal, C., III; Shakespeare, W.; Wang, Y.; Keenan, T.; Sundaramoorthi, R.; Bohacek, R.; Weigele, M.; Sawyer, T *Chem. Biol. Drug Des.* **2006**, *67*, 46.
(38) Noronha, G.; Cao, J.; Chow, C.; Dneprovskaia, E.; Hwang, L.; Lohse, D.; Mak, C. C.; McPherson, A.; Fine, R. M.; Kang, X.; Klebansky, B.; Palanki, M. S. S.; Pathak, V. P.; Renick, J.; Soll, R.; Zeng, B. In *Frontiers in Drug Design and Discovery*; Caldwell, G. W., Atta-ur-Rahman, Player, M. R., Choudhary, M. I., Eds.; Bentham Science Publishers: Oak Park, IL, 2007; Vol. 3, pp121–144.
(39) Compound **5** was evaluated in YES biochemical assay and found to be a potent inhibitor ($K_i = 0.63$ nM). The K_i value for compound **5** in VEGFr2 was 6.79 nM, and in Src it was 9.23 nM.
(40) Saint-Geniez, M.; D'Amore, P. A. Development and pathology of the hyaloid, choroidal and retinal vasculature. *Int. J. Dev. Biol.* **2004**, *48*, 1045–1058.
(41) Aguilar, E.; Scheppke, L.; Dorrell, M.; Hood, J.; Dellamary, L.; Yee, S.; Friedlander, M. Topically Applied Src Kinase/VEGFR Prodrug Reduces Retinal Vascular Permeability. Presented at the Annual Meeting of the Association for Research in Vision and Ophthalmology (ARVO), Fort Lauderdale, FL, April 3 through May 4, 2006.
(42) Attar, M.; Shen, J.; Ling, K, J.; Liu, D. T. Ophthalmic drug delivery considerations at the cellular level: drug-metabolising enzymes and transporters. *Expert Opin. Drug Delivery* **2005**, *2*, 908–891.
(43) Ahmed Kousba,A.; Yu, J.; Dellamary, L.; White, R.; Hu, S.; Tabak, A.; Cao, J.; Mak, C. C.; Renick, J.; McPherson, A.; Zeng, B.; Pathak, V.; Ibanez, G.; Stoughton, S.; Olafson,T.; Soll, R.; Doukas, J.; Hood, J.; Noronha, G.; Martin. M. Bioactivation and Ocular Disposition of Topically Applied Prodrug TG100801. Presented at the 8th Scientific Meeting of the Association for Ocular Pharmacology and Therapeutics, San Diego, CA, February 9–11, 2007.
(44) It is very difficult to accurately dissect sclera and choroid separately in the eyes of mice. Hence, we measured the concentration of the compound from the combined sclera and choroid tissues.
(45) We examined the distribution of radiolabeled compound **12** in rabbit upon topical instillation in a single eye. The compound was present in most of the removed eye tissues and distributed in various parts of the eye as anticipated. The radiolabeled material was not present in systemic circulation or any other tissues. The bulk of the compound was excreted in the feces. It appears most of the compound was drained through the nasolacrimal drainage system. Manuscript is in preparation.
(46) Miller, H.; Miller, B.; Ryan, S. J. The role of the retinal pigmented epithelium in the involution of subretinal neovascularization. *Invest. Ophthalmol. Visual Sci.* **1986**, *27*, 1644–1652.
(47) Dobi, E. T.; Puliafito, C. A.; Destro, M. A new model of choroidal neovascularization in the rat. *Arch. Ophthalmol.* **1989**, *107*, 264–269.
(48) Soubrane, G.; Cohen, S. Y.; Delayre, T.; Tassin, J.; Hartmann, M.-P.; Coscas, G. J.; Courtois, Y.; Jeanny, J.-C. Basic fibroblast growth factor experimentally induced choroidal angiogenesis in the minipig. *Curr. Eye Res.* **1994**, *13*, 183–195.
(49) Kimura, H.; Sakamoto, T.; Hinton, D. R.; Spee, C.; Ogura, Y.; Tabata, Y.; Ikada, Y.; Ryan, S. J. A new model of subretinal neovascularization in the rabbit. *Invest. Ophthalmol. Visual Sci.* **1995**, *36*, 2110–2119.
(50) (a) Lima e Silva, R.; Kachi, S.; Akiyama, H.; Shen, J.; Hatara, M. C.; Aslam, S.; Gong, Y. Y.; Khu, N. H.; Lauer, T. W.; Hackett, S. F.; Marton, L. J.; Campochiaro, P. A. Trans-scleral delivery of polyamine analogs for ocular neovascularization. *Exp. Eye Res.* **2006**, *83*, 1260–1267. (b) Umeda, N.; Kachi, S.; Akiyama, H.; Zahn, G.; Vossmeyer, D.; Stragies, R.; Campochiaro, P. A. Suppression and regression of choroidal neovascularization by systemic administration of an alpha5beta1 integrin antagonist. *Mol. Pharmacol.* **2006**, *69*, 1820–1828. (c) Nambu, H.; Nambu, R.; Melia, M.; Campochiaro, P. A. Combretastatin A-4 phosphate suppresses development and induces regression of choroidal neovascularization. *Invest. Ophthalmol. Visual Sci.* **2003**, *44*, 3650–3655. (d) Takahashi, K.; Saishin, Y.; Saishin, Y.; Mori, K.; Ando, A.; Yamamoto, S.; Oshima, Y.; Nambu, H.; Melia, M. B.; Bingaman, D. P.; Campochiaro, P. A. Topical nepafenac inhibits ocular neovascularization. *Invest. Ophthalmol. Visual Sci.* **2003**, *44*, 409–415.
(51) Private communication from Professor Martin Friedlander. Manuscript is in preparation.
(52) Calalb, M.; Zhang, X.; Polte, T.; Hanks, S. Focal adhesion kinase tyrosine-861 is a major site of phosphorylation by Src. *Biochem. Biophys. Res. Commun.* **1996**, *228*, 662–668.
(53) Lim, Y.; Han, I.; Jeon, J.; Park, H.; Bahk, Y.; Oh, E. Phosphorylation of focal adhesion kinase at tyrosine 861 is crucial for ras transformation of fibroblasts. *J. Biol. Chem.* **2004**, *279*, 29060–29065.
(54) Eliceiri, B.; Paul, R.; Schwartzberg, P.; Hood, J. D.; Leng, J.; Cheresh, D. Selective requirement for Src kinases during VEGF-induced angiogenesis and vascular permeability. *Mol. Cell* **1999**, *4*, 915–924.
(55) Abu-Ghazaleh, R.; Kabir, J.; Jia, H.; Lobo, M.; Zachary, I. Src mediates stimulation by vascular endothelial growth factor of the phosphorylation of focal adhesion kinase at tyrosine 861, and migration and anti-apoptosis in endothelial cells. *Biochem. J.* **2001**, *360*, 255–264.
(56) Eliceiri, B. P.; Puente, X. S.; Hood, J. D.; Stupack, D. G.; Schlaepfer, D. D.; Huang, X. Z.; Sheppard, D.; Cheresh, D. A. Src-mediated coupling of focal adhesion kinase to integrin alpha. (v)beta5 in vascular endothelial growth factor signaling. *J. Cell Biol.* **2002**, *157*, 149–160.
(57) http://www.clinicaltrials.gov/ct/show/NCT00509548?order=1.
(58) Doukas, J.; Mahesh, S.; Umeda, N.; Kachi, S.; Akiyama, H.; Yokoi, K.; Cao, J.; Chen, Z.; Dellamary, L.; Tam, B.; Racanelli-Layton, A.; Hood, J.; Martin, M.; Noronha, G.; Soll, R.; Campochiaro, P. A. Topical administration of a multi-targeted kinase inhibitor suppresses choroidal neovascularization and retinal edema. *J. Cell Physiol.* **2008**, *215*, accepted for publication.
(59) Verbeke, G.; Molenberghs, G. *Linear Mixed Models for Longitudinal Data*; Springer-Verlag Inc.: New York, 2000; pp 93–120.

JM7011276